View metadata, citation and similar papers at core.ac.uk
brought to you by CORE
provided by UPCommons. Portal del coneixement obert de la UPC

Projecte Fi de Carrera

Enginyeria Industrial

MODELING OF HEAT TRANSFER DURING CRYSTALLIZATION AT LOW TEMPERATURES WITH INDUCTION HEATING

Authors: Núria Espinar Lacueva

Advisor: Aleksandar Ostrogorsky

September 2010

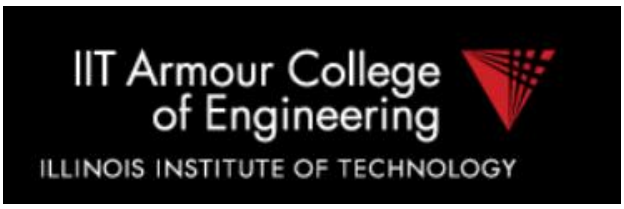

INDEX

1. Introduction

Indium iodide is a semiconductor that has a high photon stopping power for X- and gamma-rays. Although only a few investigations have been made with this material, it has been proved that the photon stopping efficiency of indium iodide crystals can be compared to that of CdTe. There are many other X- and gamma-ray detectors, but indium and iodine are less toxic than these other materials, and that is why InI has a lower risk of environmental pollution.

One of the methods that permits to obtain InI crystals is the Czochralski crystal growth technique. The Czochralski method is a common technology for growing high-quality single crystals. The Czochralski system includes various modes of heat transport and a complex range of fluid dynamic phenomena. In this configuration, an inductive heating system is frequently used to produce heat in the crucible. This crucible is heated inductively and directly by Joule's heat of eddy current induced by a high-frequency current in the coil. This internal heat generation is partly conducted into the melt and partly transferred to the surroundings.

The aim of this work is to simulate the InI crystal growth using the Czochralski method, trying to reproduce the physical conditions of the space where the experiment would take place, in order to be able to compare the results of future experimentations to the theoretical results obtained with the simulation.

The geometry will be optimized to obtain the appropriate distribution of temperatures in the melt.

At first the electromagnetic field created will be studied. Then the temperature distribution for the whole system and the velocity of the melt will be calculated.

Of specific interest are the thermal gradients in the melt and in the growing crystal, and the influence of the rotation of the crystal on the movement of the melt. The radial and axial velocities of the melt under the crystal obtained with the simulation will be compared to the theoretical velocities that would be obtained with the same material and the same rotation rate when using an infinite rotating disk.

2. Indium Iodide

Indium monoiodide (InI) is a compound semiconductor with a high atomic number (Z_{In}:49 and Z_I:53) and high density (5.31 g/cm^3). InI has a relatively low melting point (351ºC) and exhibits no solid-solid phase transition between its melting point and room temperature. Therefore, high quality InI crystals can be obtained by using simple melt-based process. InI is a brown-to-red solid that melts to a darker-colored liquid and becomes black at the boiling point.

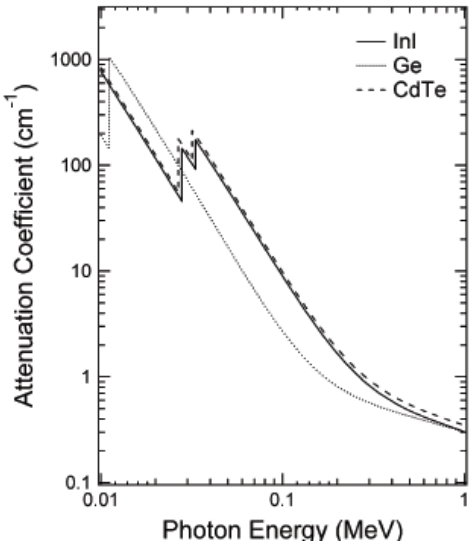

Figure 1. Attenuation coefficient for InI, Ge and CdTe as a function of photon energy [1].

InI detectors exhibit a high photon stopping power for X- and gamma-rays. As can be observed in Figure 1, the photon stopping efficiency of InI is much higher than that of Ge and compares with that of CdTe. InI has a wide band gap energy (2.0 eV) which suppresses the thermal excitation of carriers and hence permits InI detectors to have low-noise performance at room temperature.

Other compound semiconductors used for fabrication of radiation detectors consist of toxic materials such as Cd (CdTe), Hg (HgI), Pb (PbI), As (GaAs) and Tl (TlBr). Therefore there is a possibility of occupational poisoning and environmental pollution during the detector fabrication and detector handling processes. As In and I are not toxic, low risk of environmental pollution is one of the attractive properties of InI radiation detectors.

In view of these promising characteristics, InI has been studied as a material for room temperature X- and gamma-ray detectors and photodetectors for scintillators. Although InI is one of the promising materials for radiation detector fabrication, only a few investigations have been made. Furthermore, in all reported studies, the crystals were grown by the vertical Bridgman process [1-3]. So far, no attempts have been reported to grow InI using the Czochralski process.

3. Czochralski method

The Czochralski (CZ) method is the most important technique for growing high quality single crystals. The material to be grown is initially melted in a crucible located in a furnace. Due to the phase change, a crystal grows when it is vertically pulled. A seed crystal is lowered into the liquid. The temperature of the melt is adjusted so that the temperature at the center of the surface of the melt reaches the freezing point of the material. The seed crystal is slowly rotated and withdrawn and the crystal starts to grow.

The diameter of the crystal is controlled by adjusting the melt temperature and the pulling speed. A successful growth requires the control of heat and mass transport in all media. Seed rotation is used to improve the thermal symmetry and to drive forced convection in the melt.

The Czochralski process has many advantages including:

- The crystals are not restricted by the crucible walls during growth and cool down.
- The level of forced convection in the melt is easy to control.
- Seeding and growth can be observed

In the present study, an inductive heating radio frequency system is used to produce heat in the graphite susceptor.

There are two conditions that should be accomplished when growing crystals with the CZ method:

- The temperature distribution in the melt should be such that the temperature at the solid-liquid interface is the lowest in the melt. Otherwise there is a strong possibility of spurious nucleation.

- The surface of the melt should be free of foreign particles and films. This implies that the surface must be protected from dust particles and flakes of material condensed on the sides and top of the growth chamber, and if necessary from the atmosphere.

In a CZ system, different types of heat transfer mechanism coexist in the growth setup. Heat transfer includes: (i) convection, conduction and radiation in the melt (in semitransparent melts); (ii) conduction and radiation within the crystal; and (iii) gas convection and radiation between the surfaces exposed to gases. Modeling of heat generation and heat and mass transfer processes during the process is essential to understand and control the crystal growth process.

The essential parts of a crystal puller are: a crucible to hold the melt, a means of heating the melt, a seed and a mechanism for producing relative motion of the seed and the melt.

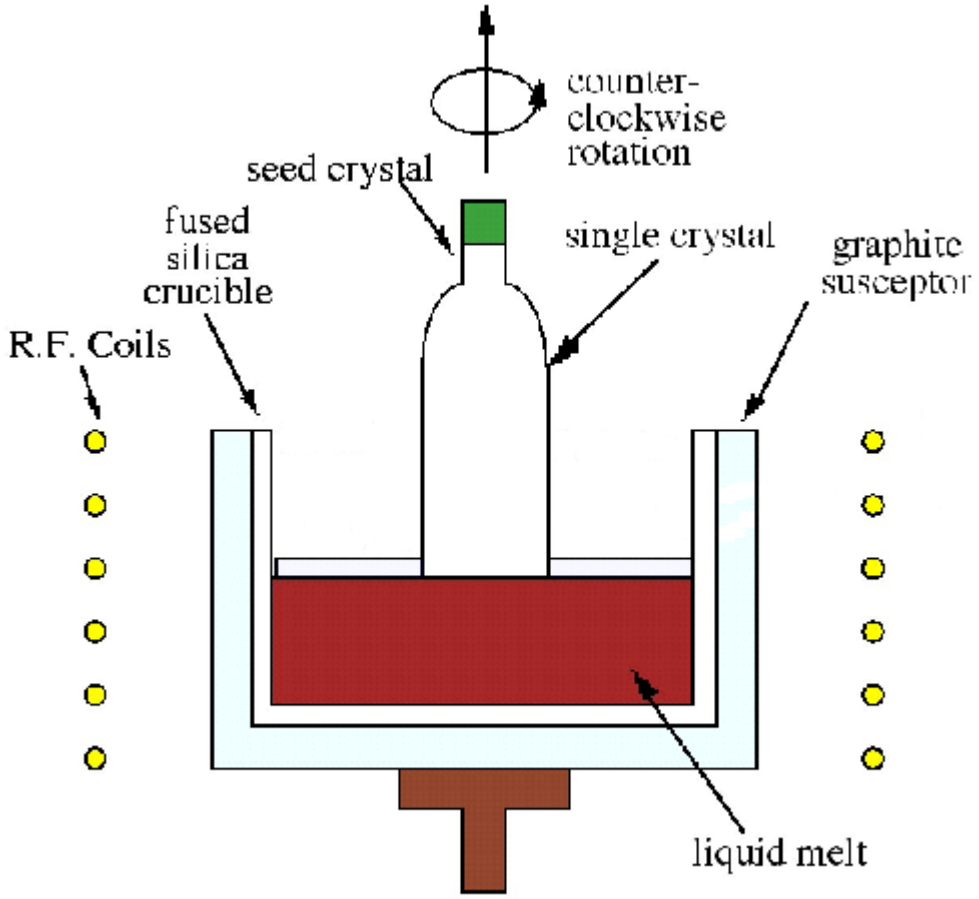

Figure 2. Schematic of Czochralski crystal grower.

4. CrysMAS

To conduct this study, the crystal growth simulation software CrysMAS is employed. This program was developed by Gerorg Mullers research team at the University of Erlangen Nurenberg and at the Fraunhofer Institute of Integrated Systems and Device Technology (IISB) in Erlangen, Germany. This package is capable of predicting high temperature heat transfer within complex crystal growth furnaces by solving the energy conservation equations using the finite volume method on an unstructured triangular grid. Radiant heat transfer calculations are implemented using view factors and an enclosure method. CrysMAS can also apply a structured grid to perform the heat transfer, fluid flow, and phase change computations within the ampoule. The solid-liquid interface is tracked to coincide with the melting-point isotherm and also sets the vertices on the appropriate boundary between the structured and unstructured mesh (of the melt and the crystal respectively).

The axial symmetry of the geometry used in the simulation allows for a simplified two-dimensional model representation in cylindrical coordinated space, with the vertical system axis assumed to be aligned with gravity.

5. Inductive heating

The principle of induction heating is frequently used in the Czochralski crystal growth technique in order to supply the required heat to the melt. This power is generated by induction heater coils that surround the crucible when an AC current is passed through the coils. This azimuthal current produces a magnetic field outside the coils which in turn generates an oscillating azimuthal electric field. Both fields penetrate the crucible, to an extent that depends in part on the electrical conductivity of the material. A parallel current flow is caused the electric field within the crucible walls. The product of the electric field strength with the current describes the rate of energy dissipation in the metal. This internal heat generation is partly conducted into the melt (at the inner wall and bottom) and partly lost to the surroundings.

The skin depth is the measure of the field penetration depth into the conductors.

$$\delta = \left(\frac{\rho}{\pi \mu \nu} \right)^{1/2} \tag{1}$$

where $\rho[\Omega m]$ is the resistivity of the material, $\mu[H/m]$ is the magnetic permeability and $\nu[Hz]$ is the frequency.

The following assumptions are commonly used in CrysMAS in the numerical calculation of induction heating:

i) The system is axi-symetric.
ii) All materials are isotropic and nonmagnetic and have no net electric charge.
iii) The displacement current is neglected.
iv) The distribution of electrical current (also voltage) in the coil is uniform.
v) The self-inductance effect in the coil is taken into account.

Under these assumptions, the governing equations are

$$\frac{\partial}{\partial r}\left(\frac{1}{r} \frac{\partial \psi}{\partial r} \right) + \frac{\partial}{\partial z}\left(\frac{1}{r} \frac{\partial \psi}{\partial z} \right) = -\mu_0 J_\phi \tag{2}$$

where

$J_\phi = J_0 \cos(\omega t)$ in the coil, and

$J_\phi = -\frac{\sigma}{r} \frac{\partial \psi}{\partial t}$ in the conductors (3)

with a solution of the form

$$\psi(r,z,t) = C(r,z)\cos(\omega t) + S(r,z)\sin(\omega t) \tag{4}$$

and

$$Q(r,z)=\frac{\sigma\omega^{2}}{2r^{2}}\left(C^{2}+S^{2}\right) \tag{5}$$

where $\psi(r,z,t)\left[Wb\right]$ is the magnetic stream function; $C(r,z)\left[Wb\right]$ and $S(r,z)\left[Wb\right]$ the in-phase and out-of phase components, respectively; $Q(r,z)\left[W/m^{3}\right]$ the volumetric generation in the crucible; $\omega\left[Hz\right]$ the frequency of the electrical current in the induction coil; $J_{\phi}\left[A/m^{2}\right]$ the charge current density; $\sigma\left[S/m\right]$ the electrical conductivity; $\mu_{0}\left[H/m\right]$ the magnetic permeability of free space; and $t\left[s\right]$ the time. The boundary conditions are $\psi=0$, both in the far field ($r,z\rightarrow\infty$) and at the axis of symmetry ($r=0$).

It is assumed that the electromagnetic field is independent of the temperature of the crucible. Under this assumption, the induction problem is solvable independently.

The frequency in the coil will be 1.5MHz, and the intensity will vary in order to obtain the freezing point temperature in the interface between the crystal and the melt.

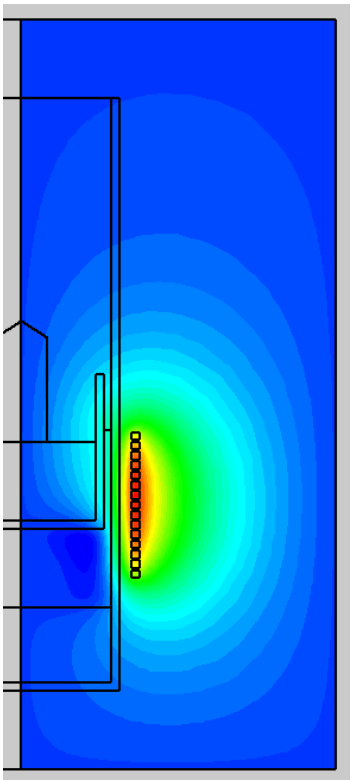

Figure 3. Magnetic field in the system studied.

6. Geometry and properties of the materials

The aim of the project is to simulate the Czochralski process when using the materials and devices available in the laboratory where the experiment would take place. A schematic diagram of the apparatus is shown in Figure 4, and in Figure 5 one can observe the material of each part.

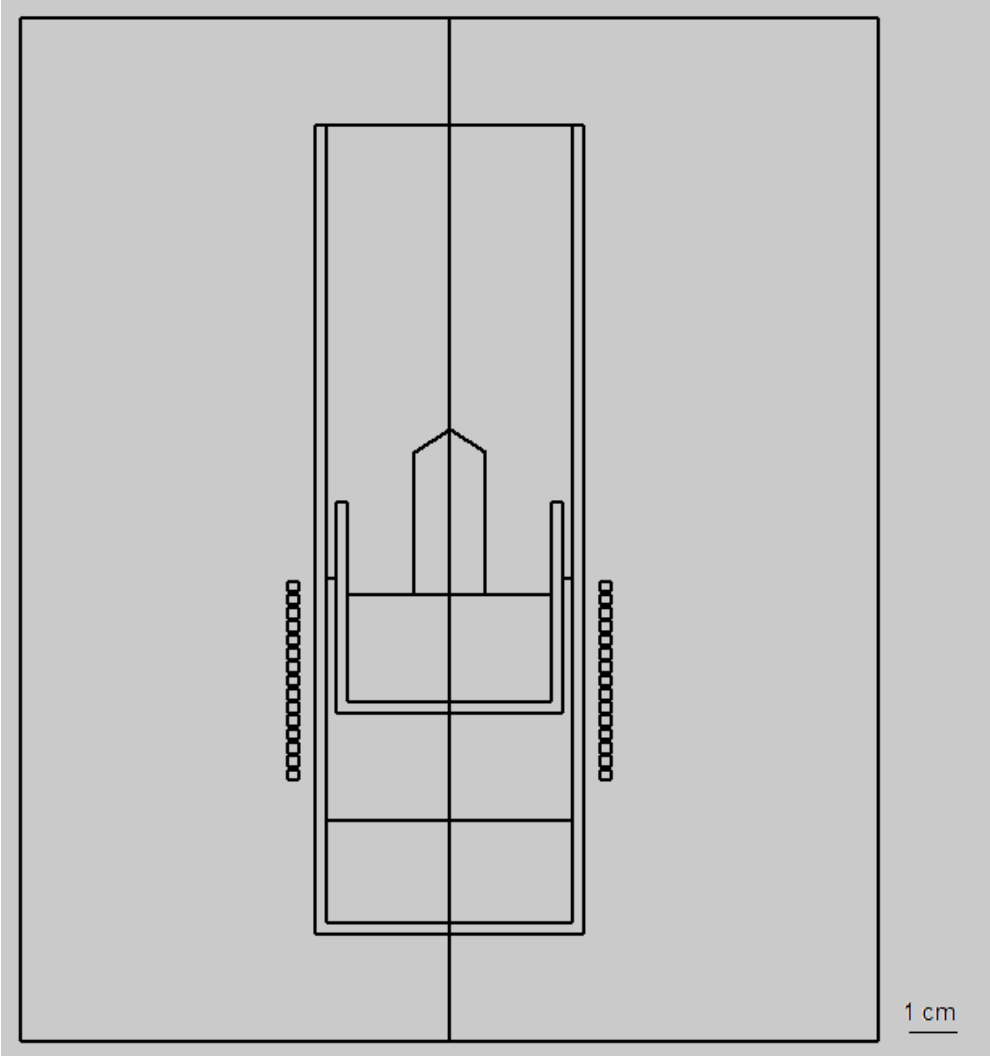

Figure 4. Geometry of the Czochralski crystal grower used for the simulation.

Crystal diameter = 1.2cm

Melt height = 2cm

Crucible diameter = 4cm

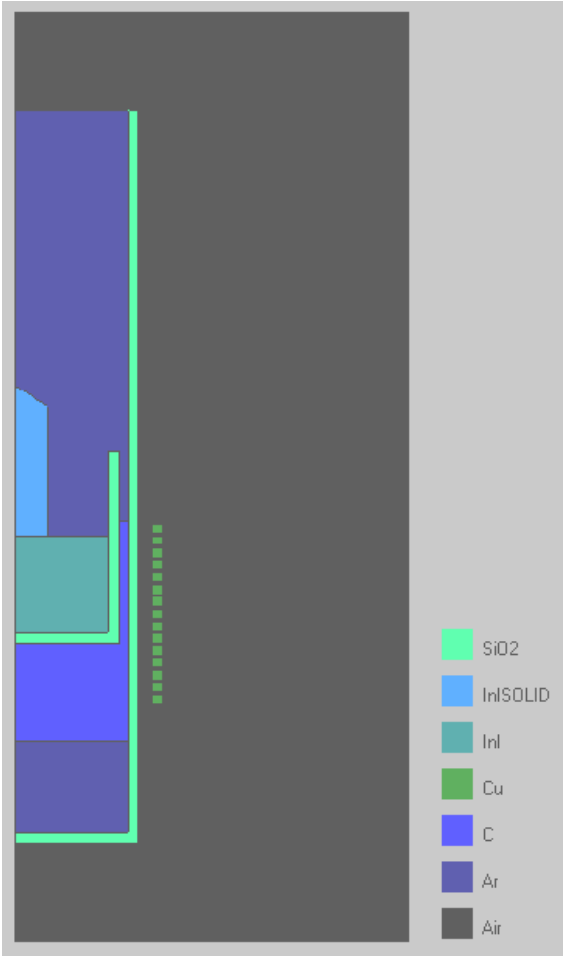

Figure 5. Materials assignment to each part of the geometry.

The melt is contained in a quartz crucible. This crucible is surrounded by a graphite support and a quartz support. The piece made from graphite is heated by inductive heating and transmits the heat to the melt (graphite is the only material with an important electrical conductivity).

Table 1 shows the properties of the materials used in the experiment.

Material	ρ (kg/m^3)	σ (S/m)	Cp (J/kg·K)	k (W/m·K)	Transparency	ε	Transparent windows (μm)	μ (kg/m·s)	β (1/K)	α (m^2/s)
Air	1	0	1006	0.024	Transparent	1	-	-	-	-
Ar	1.622	0	520	0.030	Transparent	1	-	-	-	-
C	2000	100000	710	140	Opaque	0.9	-	-	-	-
Cu	8900	0	380	401	Opaque	1	-	-	-	-
Inl (sol)	5310	0	864	0.5	Transparent	0.9	-	-	-	-
Inl (liq)	5310	0	864	0.5	Transparent	0.9	-	0.00531	0.0001	0.158x10^{-6}
SiO_2	2650	0	743	1.4	Visibility bands	0.93	0.2 - 4.0	-	-	-

Table 1. Thermophysical properties of the materials used.

7. Optimization of the geometry and temperature field

Since InI has a low freezing point, 355ºC, low temperature gradients are expected in the melt, making the control of the process (e.g. diameter control) difficult. A key goal of this project is to have as much gradient as possible at the surface of the melt in order to have the freezing point temperature only in the center of the surface.

The graphite crucible is the one heated by the inductive currents and is also the one that transmits heat to the melt, its influence to the temperature gradient will be studied in this part. Afterwards, the most appropriate height of the graphite is chosen for the final geometry of the experiment.

"L" is defined as the distance between the surface of the melt and the top of the graphite wall. Four different values for L have been chosen: 0mm (L1), 3mm (L2), 7mm (L3) and 10mm (L4).

The values for L have been studied in five different situations, defining in all of them the melt as a solid, to avoid the effects of the movement of the liquid. These are the situations:

(1) Only the melt
(2) The melt with a crystal seed
(3) The melt with a crystal seed with a b.c. of 25ºC at the top of the seed
(4) The melt with a crystal
(5) The melt with a crystal and seed with a b.c. of 25ºC at the top of the seed

In the following graphics, the temperature at the surface of the melt is represented in function of the radius.

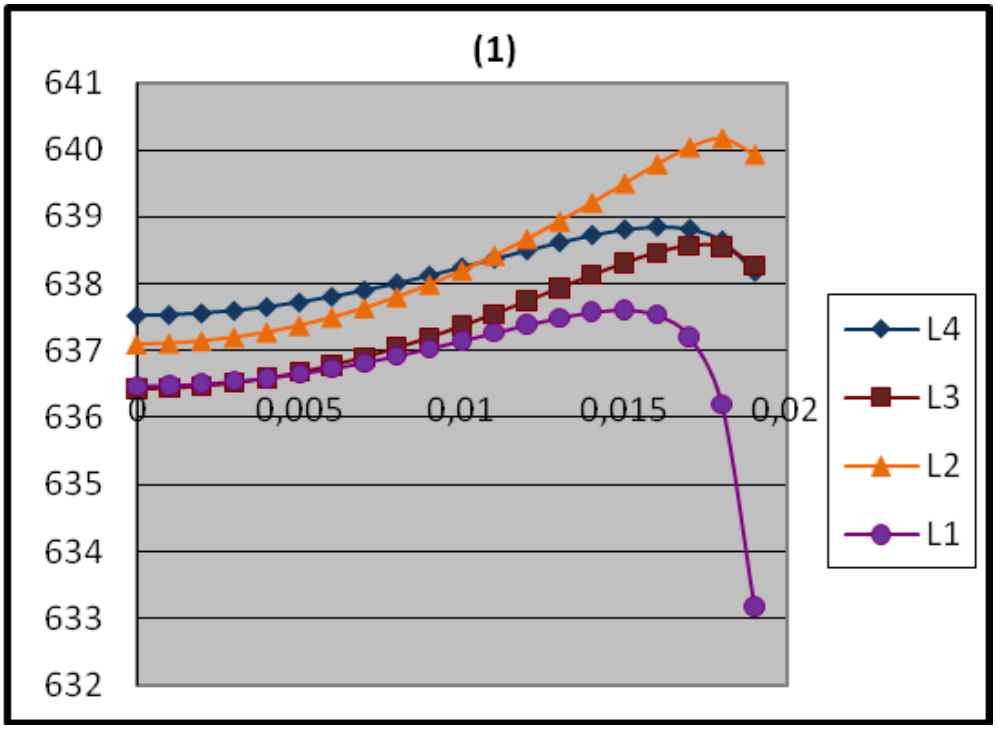

Figure 6. Temperatures profile at the surface of the melt without a seed or a crystal.

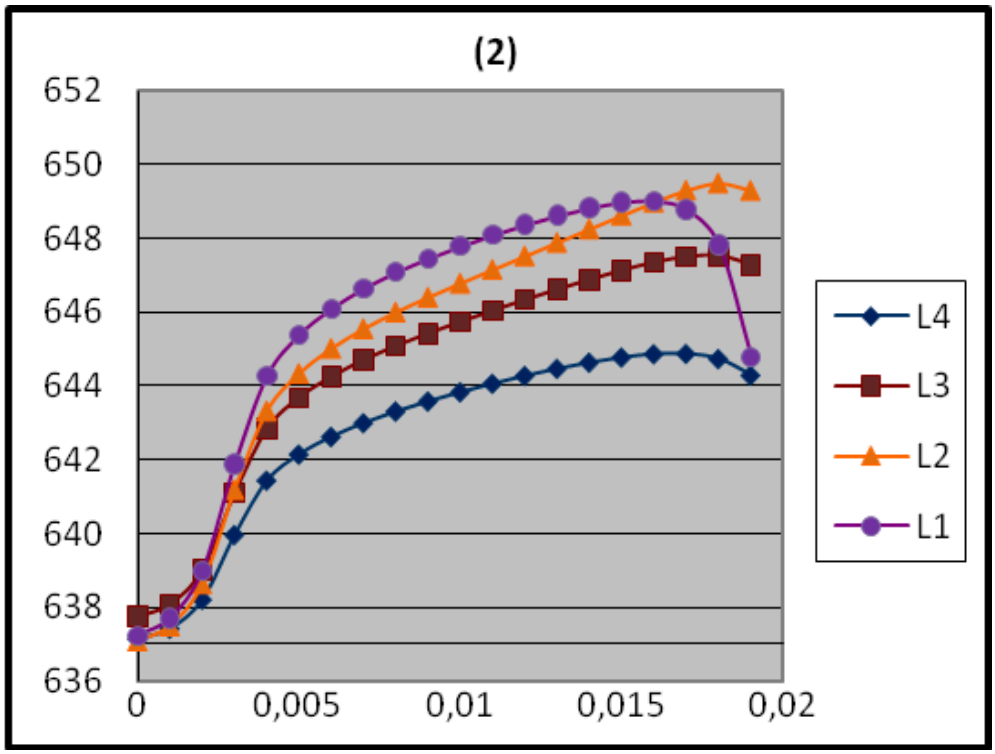

Figure 7. Temperatures profile at the surface of the melt when there is a crystal seed.

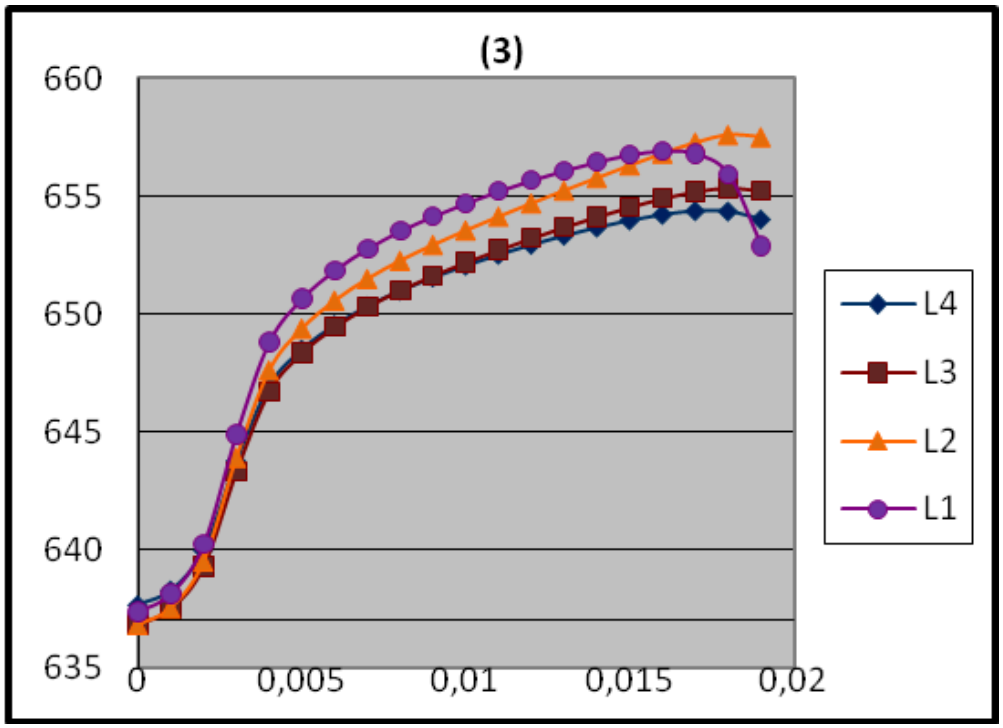

Figure 8. Temperatures profile at the surface of the melt when there is a crystal seed and 25ºC at the top of the seed.

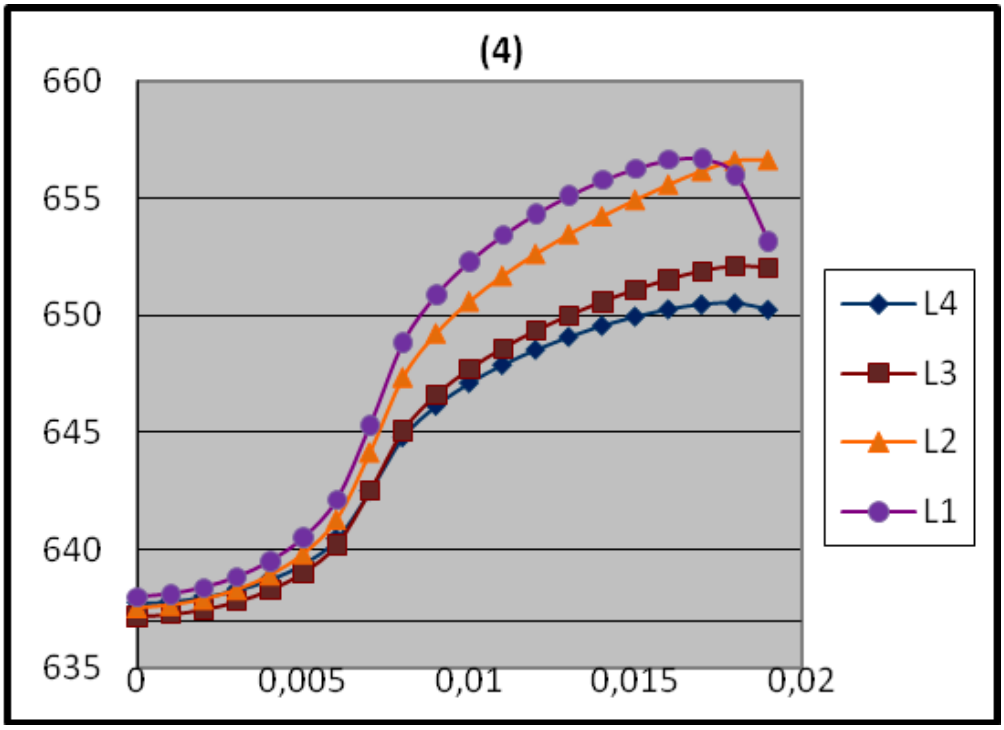

Figure 9. Temperatures profile at the surface of the melt when there is a crystal.

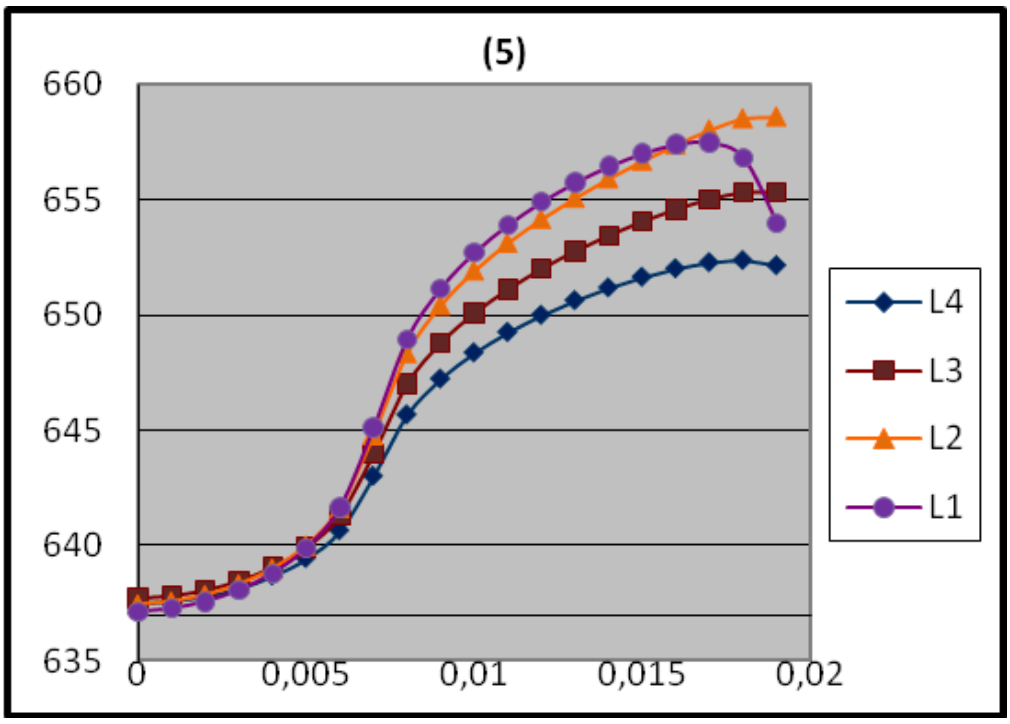

Figure 10. Temperatures profile at the surface of the melt when there is a crystal and 25ºC at the top of the crystal.

Observing the graphics, one can see that the size for L that produces the maximum gradient in the melt is de L=3mm, which is the length of L finally chosen as it is showed in the previous section (geometry).

8. Mathematic model and Nondimensional parameters

In a CZ system, heat transfer includes convection, conduction and radiation within the melt, conduction and radiation within the crystal and gas convection and radiation between exposed surfaces.

For the temperature and flow field calculation this model involves the following assumptions:

i) The system is in quasi-steady state
ii) The system is axially symmetric
iii) The melt is incompressible Newtonian fluid

A realistic model will be obtained if the nondimensional parameters of the model are set equal to nondimensional parameters of the growth process. The nondimensional parameters relevant to convection in Czochralski melts appear in the governing equations.

Continuity:

$$\nabla \cdot V^* = 0 \tag{6}$$

Navier-Stokes:

$$\frac{\partial V^*}{\partial t} + \left(V^* \cdot \nabla\right) V^* = -\nabla p + \frac{1}{\mathrm{Re}} \nabla^2 V^* + \frac{Gr}{\mathrm{Re}^2} \theta e \tag{7}$$

Energy conservation:

$$\frac{\partial \theta}{\partial t} + \left(V^* \cdot \nabla\right) \theta = \frac{1}{\mathrm{Re}\,\mathrm{Pr}} \nabla^2 \theta \tag{8}$$

V^* and θ are the nondimensional velocity and the nondimensional temperature:

$$V^*(r,\theta,z) = \frac{V(r,\theta,z)}{\omega r} \tag{9}$$

$$\theta(r,\theta,z) = \frac{T(r,\theta,z) - T_C}{T_H - T_C} \tag{10}$$

V is the dimensional velocity, T is the dimensional temperature, T_C and T_H are the lowest and the highest temperatures in the melt, r is the crystal radius, ω is the rotation rate of the crystal, ∇p is the gradient of the nondimensional dynamic pressure, and e is the axial unit vector. Re, Gr and Pr are the nondimensional parameters that need to be set equal.

Reynolds number:

$$\mathrm{Re} = \frac{\omega r^2}{\nu} = \frac{\omega r^2 \rho}{\mu} \tag{11}$$

Grashof number:

$$Gr = \frac{g\beta\Delta T r_c^{\,3}}{\nu^2} = \frac{g\beta\Delta T r_c^{\,3}\rho^2}{\mu^2} \tag{12}$$

Prandtl number:

$$\Pr = \frac{\nu}{\alpha} = \frac{\mu C_p}{k} \tag{13}$$

where $\nu\left[m^2/s\right]$ is the kinematic viscosity, $g\left[m/s^2\right]$ is the gravity constant, $\beta\left[1/k\right]$ is the volumetric expansion, $\Delta T\left[^{o}C\right]$ is the highest temperature difference in the melt, $r_c\left[m\right]$ is the crucible radius and $\alpha\left[m^2/s\right]$ is the thermal diffusivity.

In the experiment, it is necessary that the forced convection is predominant over the natural convection. This condition is accomplished when $\frac{\mathrm{Re}^2}{Gr} >> 1.$

The Reynolds number can be matched by adjusting the rotation rate, and the Grashof number can be matched by adjusting the size of the melt r_c and/or adjusting the maximum temperature difference in the melt ΔT. The size of the melt is fixed, as the crucible used is the one available in the laboratory. To obtain the previous relation, it would be interesting to have a low temperature difference in the melt. However, as it was said in a previous section, it is important to have a high gradient of temperatures to get the melting point temperature only in the center of the surface of the melt. Therefore, the parameter that can be changed to accomplish the relation mentioned is the rotation rate of the crystal.

The rotation rate of the crystal chosen will have a frequency of 2Hz. With this value, as it will be shown in the next sections, it is possible to obtain a predominant forced convection.

9. Boundary conditions, meshing, process parameters

The grid used in the simulation is showed in Figure 11.

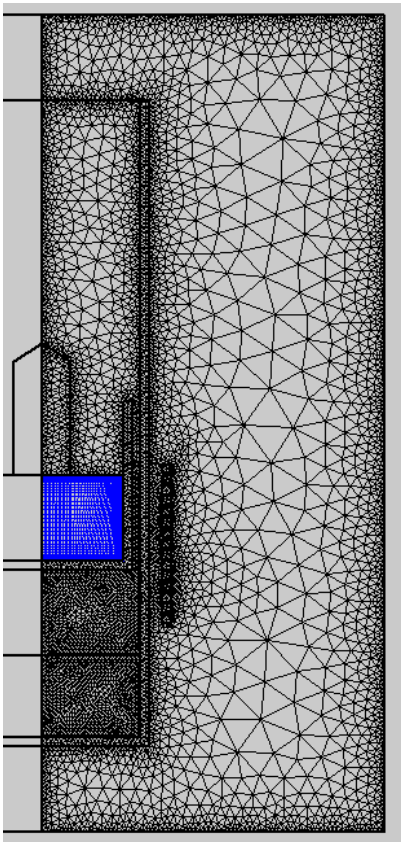

Figure 11. Grid used for the simulation

A two-dimensional mesh has been used. The size of the grid has to be the appropriate for every region. A structured mesh is applied in the melt, as it is useful when a high spatial resolution is required. Moreover, the stability of the fluid flow solution algorithm on the structured mesh is essentially higher than on the unstructured mesh.

The thermophysical boundary conditions used in the simulation are the ones that allow representing better the conditions in the laboratory where the experiment would take place.

As far as the temperature is concerned, it is set to be 300K in the far field ($r, z \to \infty$) and 323K at the top of the large quartz crucible, as it is in touch with the support structure.

In the far field, as it is explained in the Inductive Heating section, the in-phase and out-of-phase components are set to be zero.

The four physical phenomena included in the simulation are Inductive heating, Temperature, Convection (that gives the radial and axial velocities fields in the melt) and Azimuthal Flow (that gives the azimuthal velocities). At first the power distribution in the graphite crucible has been computed, and then the temperature and flow field have been calculated using this power as a source term.

10. Flow driven by buoyancy forces

First of all, it is necessary to know how the melt moves only due to the natural convection, that is to say, driven by the heat transferred from the walls of the crucible to the melt. To calculate that, the rotation rate and the pulling rate of the crystal are set to zero.

The distribution of temperatures obtained in the system is shown in Figure 12.

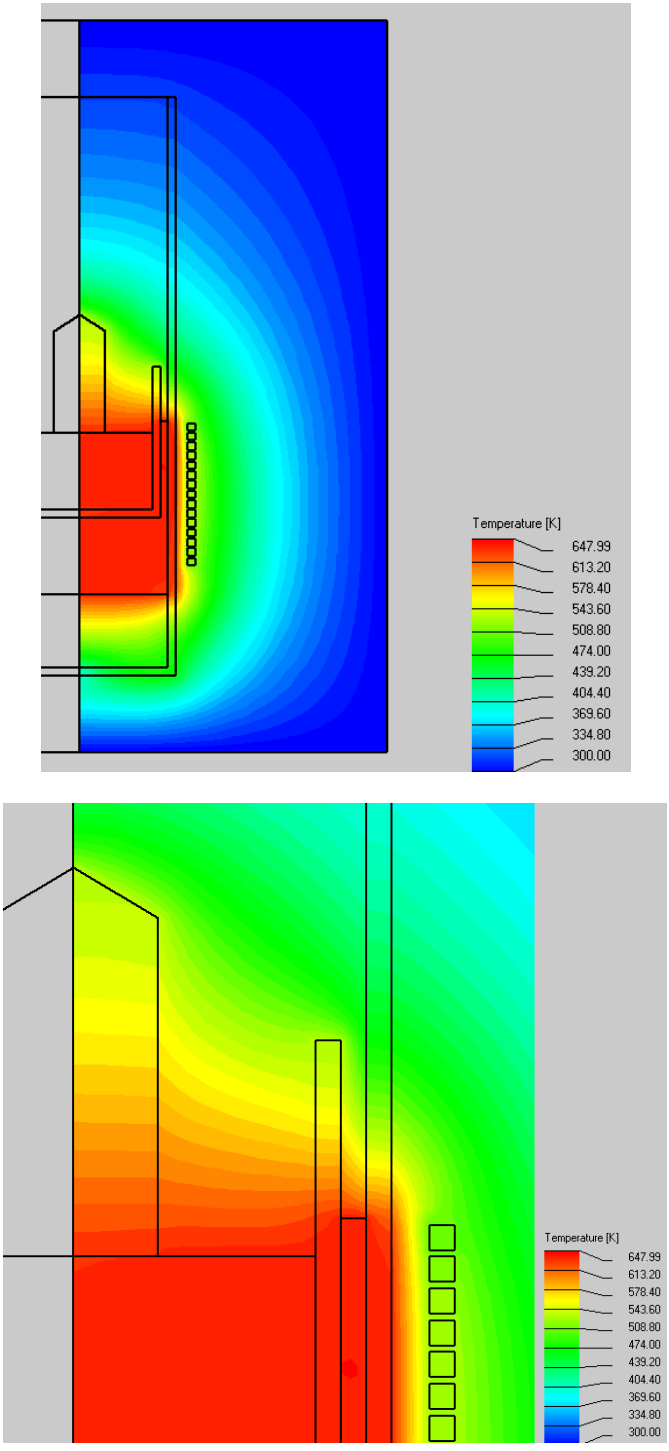

Figure 12. Distribution of temperatures when the flow is only driven by buoyancy forces.

In the following figures, one can observe the radial and axial velocities of the melt.

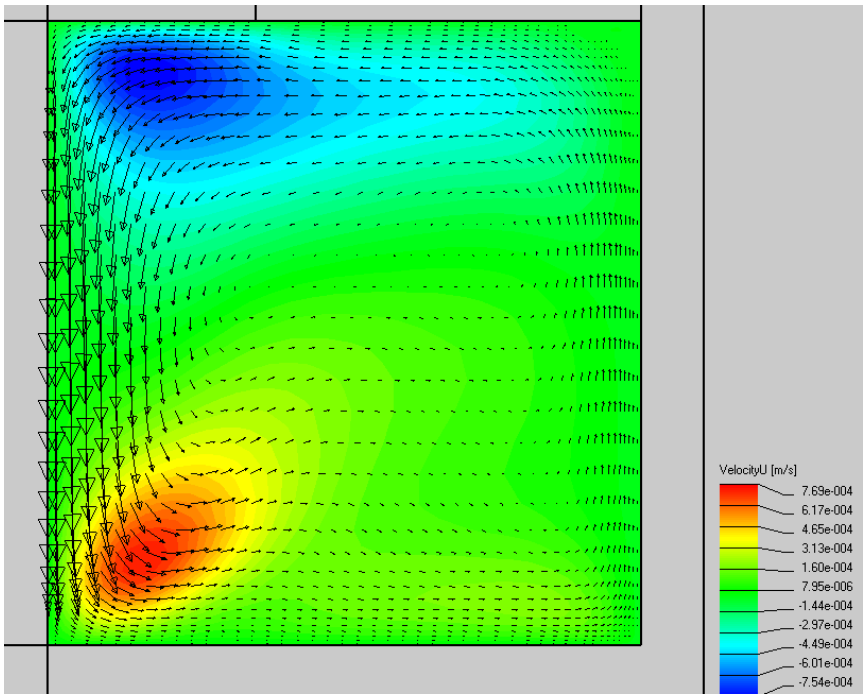

Figure 13. Radial velocities in the melt when the flow is only driven by buoyancy forces.

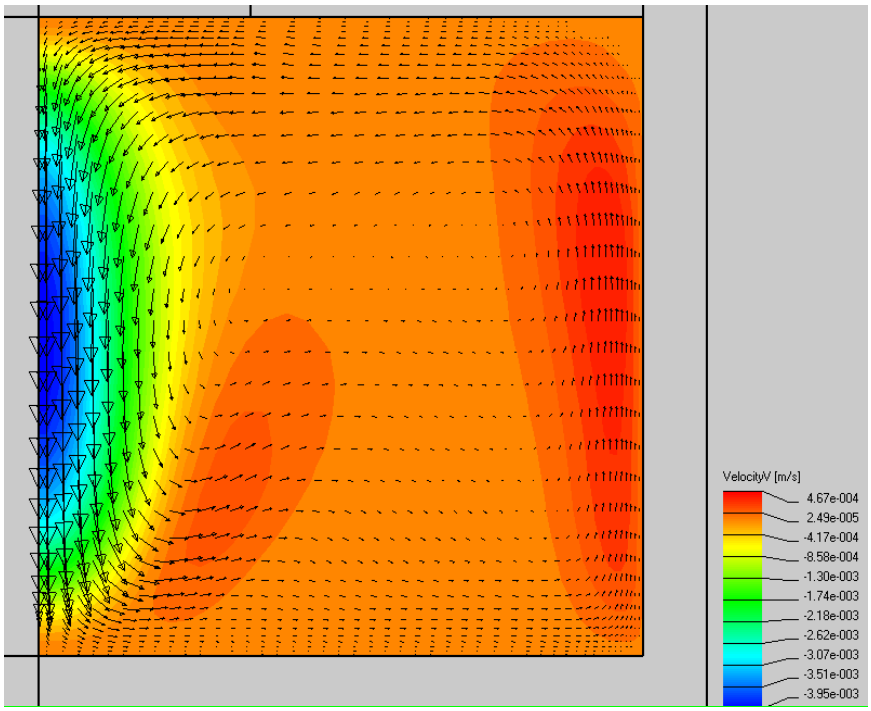

Figure 14. Axial velocities in the melt when the flow is only driven by buoyancy forces.

As expected, the flow moves upward along the crucible walls. This is because the melt expands and becomes less dense when is heated by the walls of the crucible wall. It cools down and becomes denser while flowing along the surface. Next, it flows down again through the center of the liquid region.

The Grashof number represents the ratio of the buoyancy forces to the viscous forces. The highest temperature difference is the melt is 6K. The Grashof number, using equation (12), has the following value:

$$Gr = \frac{9.81 \cdot 0.0001 \cdot 6 \cdot 0.02^3 \cdot 5310^2}{0.00531^2} = 47088$$

The maximum velocities in the melt calculated using the CrysMAS are:

$$V_{r\max} = 0.000769 m/s$$

$$V_{z\max} = 0.003950 m/s$$

corresponding to the Reynolds numbers of,

$$\mathrm{Re}_{r,\max} = \frac{V_{r\max} D\rho}{\mu} = \frac{0.000769 \cdot 0.04 \cdot \cdot 5310}{0.00531} = 30.76$$

$$\mathrm{Re}_{z,\max} = \frac{V_{z,\max} D\rho}{\mu} = \frac{0.00395 \cdot 0.04 \cdot \cdot 5310}{0.00531} = 158$$

$Re^2 << Gr$, which shows that natural convection controls the melt.

11. Flow driven by crystal rotation

This section is focused to study the melt driven by the crystal rotation, without considering the effects of the buoyancy forces. Consequently, the value of the gravity will be set to zero and the pulling rate too. The rotation of the crystal is set to a frequency of 2Hz (120rpm). This value is reasonable for the process studied and for the characteristics of the crystal and crucible used, and also permits to accomplish the relation between the Reynolds number and the Grashof number desired (explained in section 8) when the melt is under the effects of both natural and forced convection (situation studied in section 12).

The distribution of temperatures obtained in the system is shown in Figure 15.

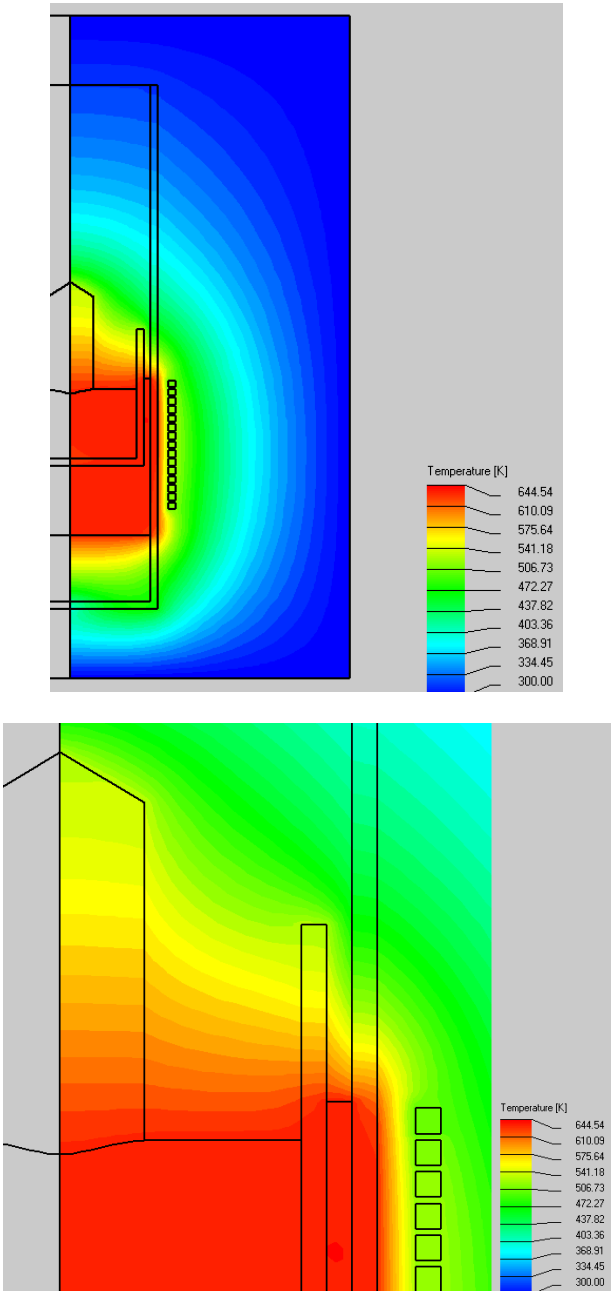

Figure 15. Distribution of temperatures when the flow is only driven by the crystal rotation.

In the following figures, one can observe the radial, axial and azimuthal velocities of the melt.

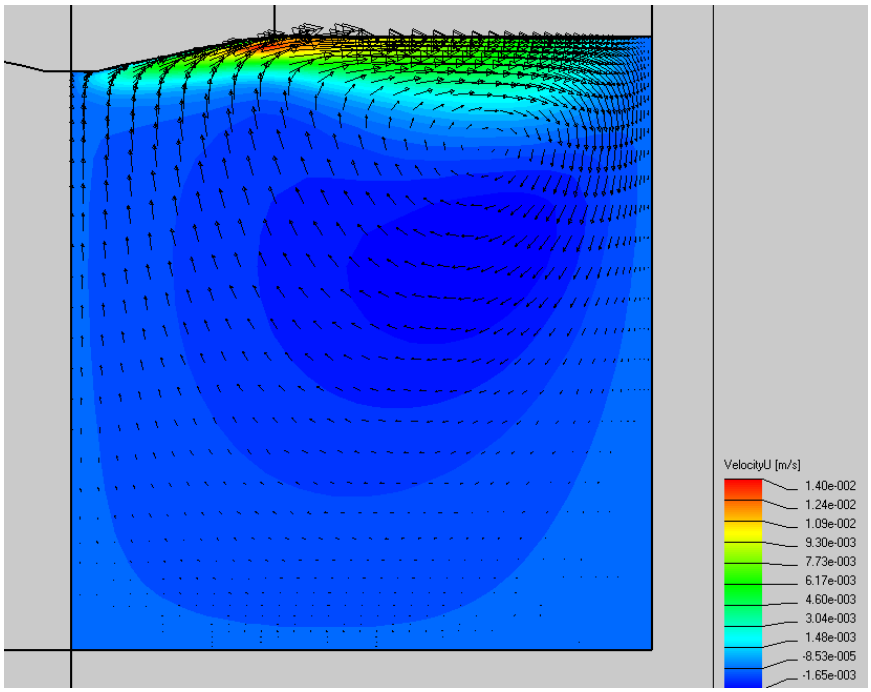

Figure 16. Radial velocities in the melt when the flow is only driven by the crystal rotation.

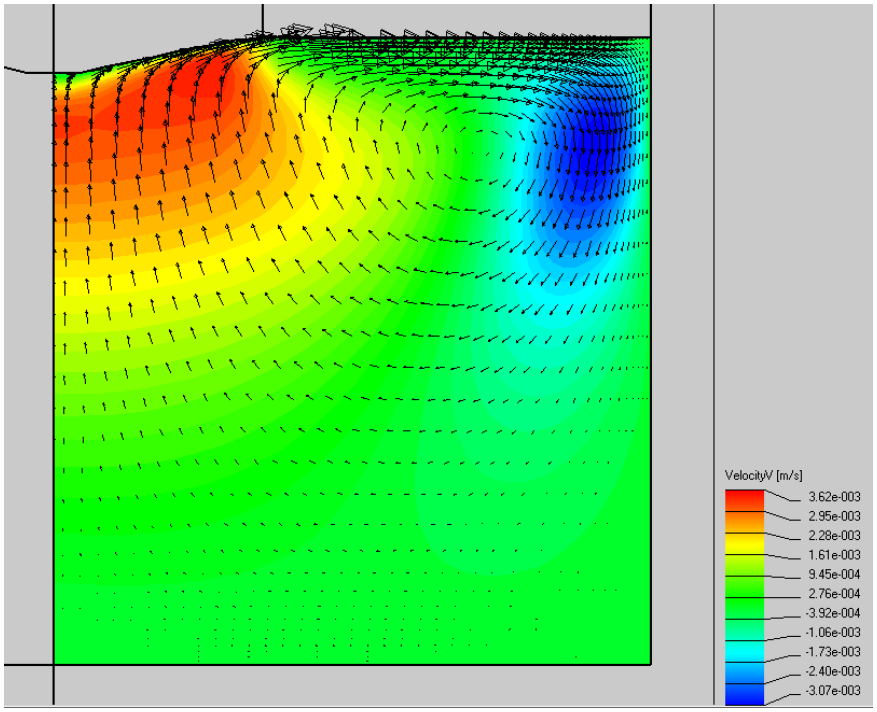

Figure 17. Axial velocities in the melt when the flow is only driven by the crystal rotation.

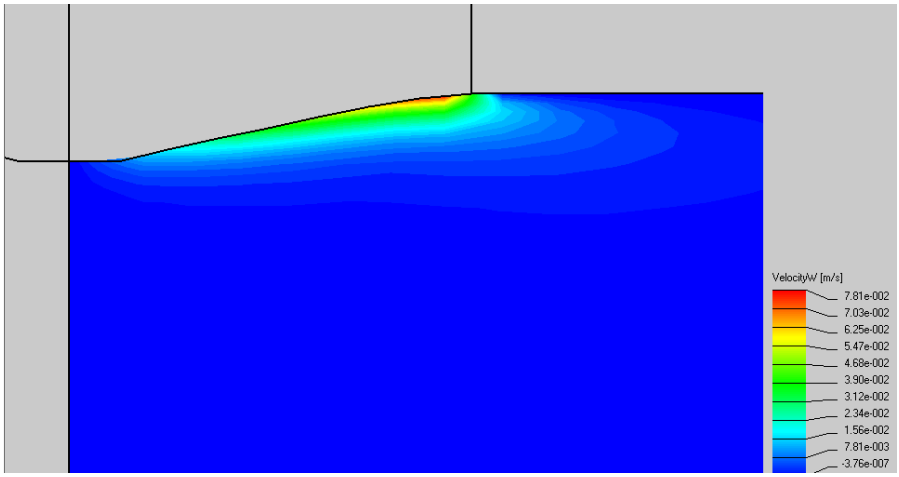

Figure 18. Azimuthal velocities in the melt when the flow is only driven by the crystal rotation.

In contrast to the previous section, the flow along the melt surface is radially outwards. This is because of the centrifugal force in the melt, introduced by rotating crystal. The centrifugal force makes the liquid at the top to move towards the walls of the crucible.

The rotation of the crystal also causes azimuthal velocity (V_θ). Only the layers of liquid next to the crystal are affected by this movement.

The Reynolds number based on the rotation rate is defined as in equation (11).

In the present study, its value is:

$$\mathrm{Re} = \frac{2 \cdot \pi \cdot 2 \cdot 0.006^2 \cdot 5310}{0.00531} = 452$$

The maximum velocities calculated using the CrysMAS are:

$$V_{r\,\max} = 0.014 m/s$$

$$V_{z\,\max} = 0.00362 m/s$$

$$V_{\theta\,\max} = 0.0781 m/s$$

Reynolds numbers based on these velocities are:

$$\mathrm{Re}_{r,\max} = \frac{V_{r\,\max} D\rho}{\mu} = \frac{0.014 \cdot 0.02 \cdot 5310}{0.00531} = 280$$

$$\mathrm{Re}_{z,\max} = \frac{V_{z,\max} D\rho}{\mu} = \frac{0.00362 \cdot 0.02 \cdot 5310}{0.00531} = 72.4$$

$$\mathrm{Re}_{\theta,\max} = \frac{V_{\theta,\max} D\rho}{\mu} = \frac{0.0781 \cdot 0.02 \cdot 5310}{0.00531} = 1562$$

Because of the melt convection, the shape of the solid-liquid interface becomes convex.

The complete geometry of the interface can be observed in Figure 19.

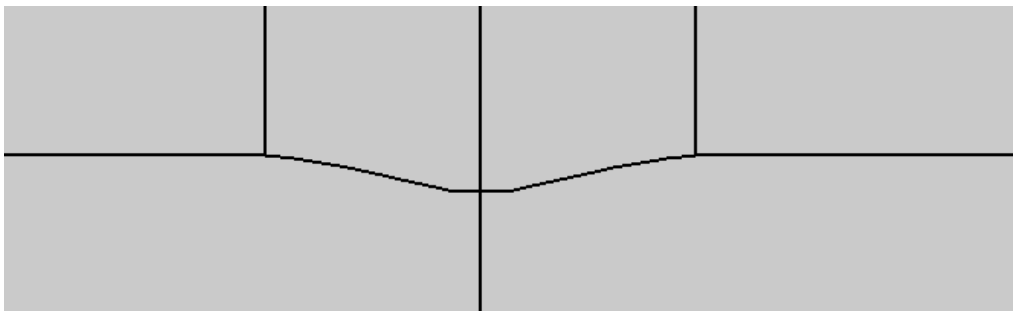

Figure 19. Geometry of the interface when the flow is only driven by the crystal rotation.

12. Combined natural and forced convection

Once both phenomena have been studied separately, the more realistic situation is considered, where the melt is submitted to both natural and forced convection, still without pulling the crystal. Consequently, the value for gravity is set again to its real value (9.81m/s^2), and the frequency of the rotation is kept at 2Hz.

In these conditions, the distribution of temperatures at the steady state is shown in Figure 20.

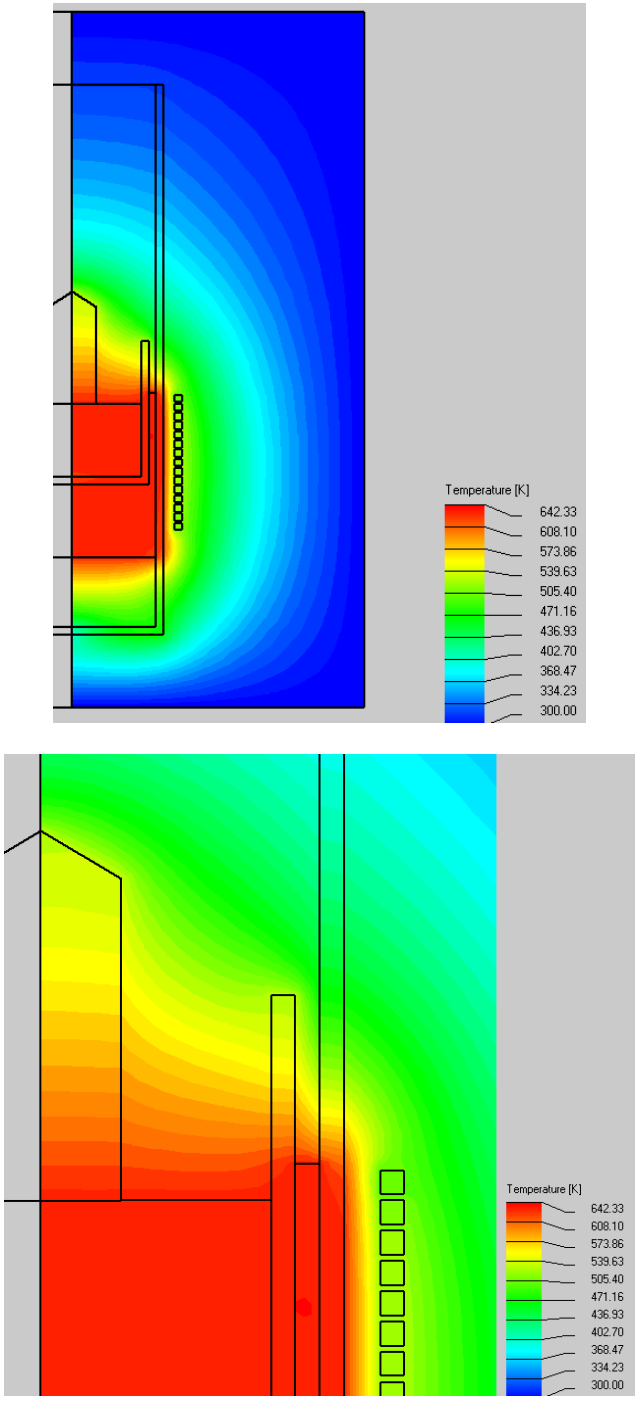

Figure 20. Distribution of temperatures when the flow is driven by both natural and forced convection.

In the following figures, one can observe the radial, axial and azimuthal velocities of the melt.

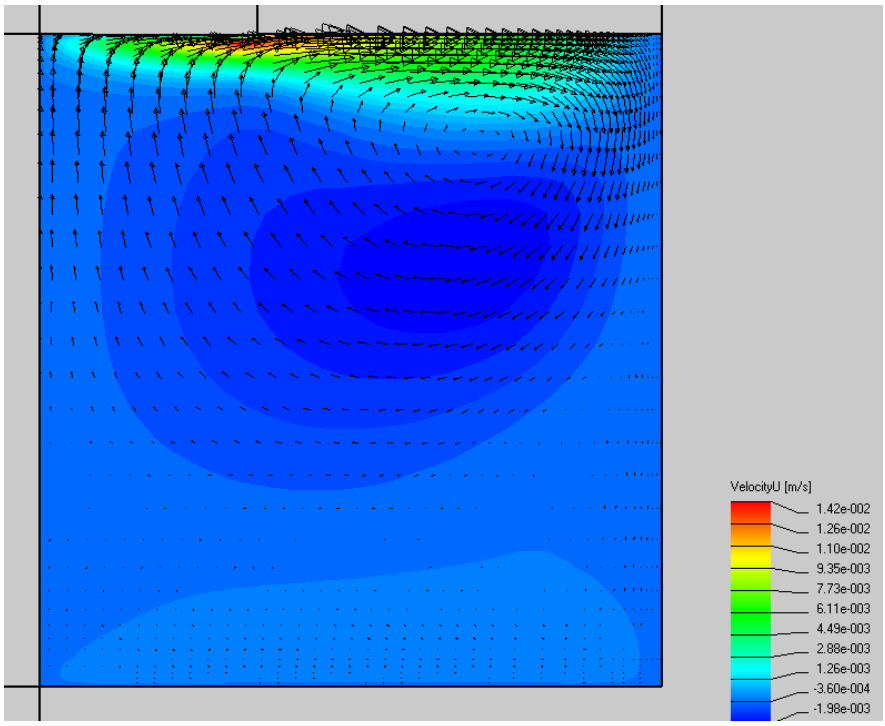

Figure 21. Radial velocities in the melt when the flow is driven by both natural and forced convection.

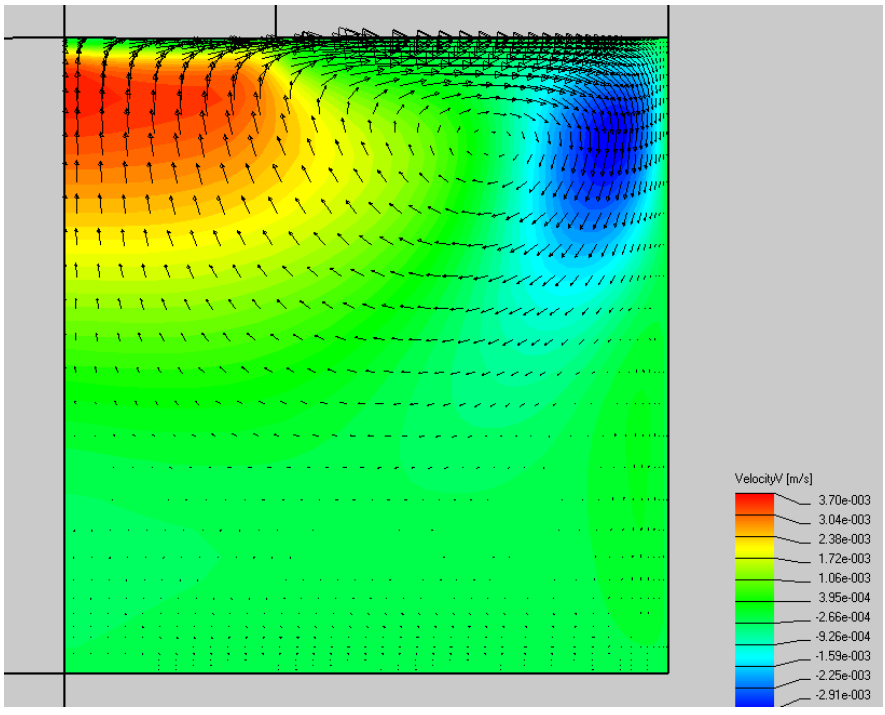

Figure 22. Axial velocities in the melt when the flow is driven by both natural and forced convection.

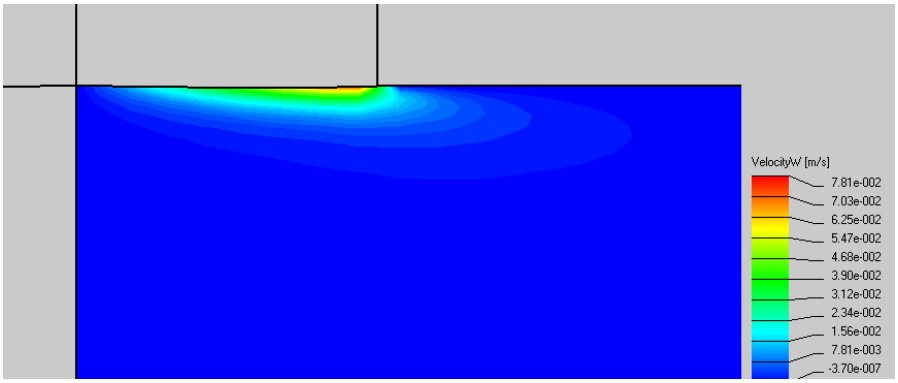

Figure 23. Azimuthal velocities in the melt when the flow is driven by both natural and forced convection.

As one can observe in the previous pictures, the flow moves outwards, fact that shows that the forced convection is predominant over natural convection.

The relative importance of the forced and natural convection can be estimated through the ratio of Re^2 and Gr numbers.

For $\frac{\mathrm{Re}^2}{Gr} >> 1$ the flow is dominated by forced convection.

The highest ΔT in the melt is 2K, so the Grashof number has the following value:

$$Gr = \frac{9.81 \cdot 0.0001 \cdot 2 \cdot 0.02^3 \cdot 5310^2}{0.00531^2} = 15696$$

The Reynolds number has the same value as in the previous case.

$$\mathrm{Re} = \frac{2 \cdot \pi \cdot 2 \cdot 0.006^2 \cdot 5310}{0.00531} = 452$$

The relation studied takes the following value:

$$\frac{\mathrm{Re}^2}{Gr} = \frac{452^2}{15696} = 13$$

confirming that the forced convection should control the melt flow.

The maximum velocities in the melt are the following ones:

$$V_{r\,\max} = 0.0142 m/s$$

$$V_{z\,\max} = 0.0037 m/s$$

$$V_{\theta\,\max} = 0.0781 m/s$$

Reynolds numbers based on these velocities are:

$$\mathrm{Re}_{r,\max} = \frac{V_{r\max} D\rho}{\mu} = \frac{0.0142 \cdot 0.02 \cdot 5310}{0.00531} = 284$$

$$\mathrm{Re}_{z,\max} = \frac{V_{z,\max} D\rho}{\mu} = \frac{0.0037 \cdot 0.02 \cdot 5310}{0.00531} = 74$$

$$\mathrm{Re}_{\theta,\max} = \frac{V_{\theta,\max} D\rho}{\mu} = \frac{0.0781 \cdot 0.02 \cdot 5310}{0.00531} = 1562$$

These values are almost the same to the ones got with only forced convection. This was expected, since Re^2>>Gr.

The natural convection does not have a significant effect on the velocity of the melt, but the changes on the interface geometry are significant. It can be observed in the previous images and in Figure 24 that the solid-liquid interface is almost flat.

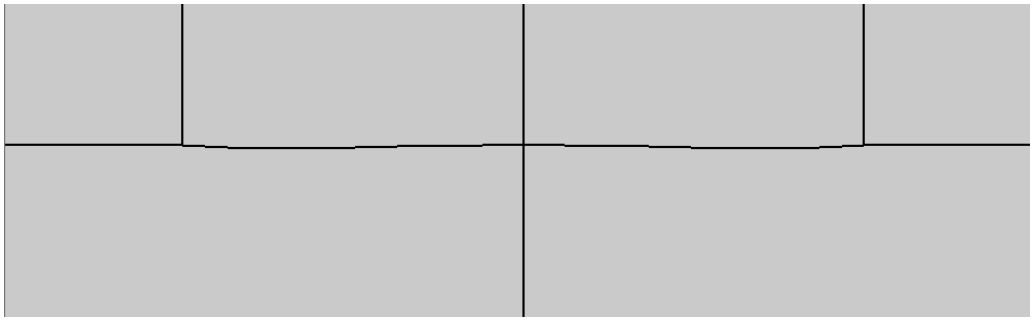

Figure 24. Geometry of the interface when the flow is driven by both natural and forced convection.

12.1. Comparison to analytical solution for the infinite rotating disk for Gr<<Re^2

Von Kármán studied the steady flow of an incompressible viscous fluid, due to rotating infinite disk. The cylindrical polar coordinates are r, θ and z; the flat disc is taken at $z = 0$ and it is rotating with constant angular velocity ω about axis $r = 0$. The motion of the fluid is considered on the side of the plane for which z is positive. The fluid is infinite in extent and $z = 0$ is the only boundary.

If V_r, V_θ and V_z are the components of the velocity of the fluid in the directions of r, θ and z, and p is the pressure, then von Kármán shows that the equations of motion and continuity are satisfied by taking

$$V_r = rf(z),\ V_\theta = rg(z),\ V_z = h(z),\ p = p(z) \tag{14}$$

The boundary conditions are $V_r = 0$, $V_\theta = \omega r$, $V_z = 0$ at $z = 0$, and $V_r = 0$, $V_\theta = 0$ at $z = \infty$. V_z does not vanish at $z = \infty$ but must tend to a finite negative limit. This means that there is a steady inflow against the rotating wall as is to be expected for reasons of continuity. Owing to the adherence of the fluid, the rotating wall acts like a kind of centrifugal fan. Next to the wall the fluid is continuously carried to the outside, to be replaced by axial inflow.

To obtain the equations in a non-dimensional form:

$$f = \omega F(\xi),\ g = \omega G(\xi),\ h = \sqrt{\omega\nu}H(\xi),\ p = \rho\nu\omega P(\xi),\ \xi = z\sqrt{\frac{\omega}{\nu}} \tag{15}$$

Cochran (1934) improved the accuracy with matched inner and outer expansions. Rogers and Lance (1960) gave very accurate numerical solutions.

In the next figure, one can find the numerical solutions for F, G, H and P.

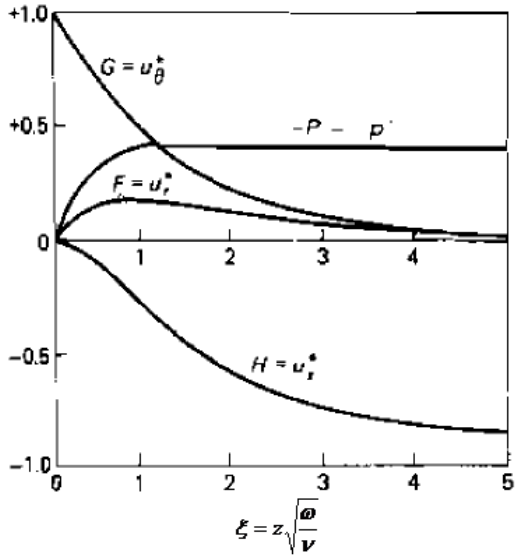

Figure 25. Numerical solutions of F, G, H and P for the infinite rotating disk [9].

The values of F, G, H and P (which are also tabulated [9]), define the velocities in the infinite melt driven by an infinite rotating disk.

In this section, the velocities in the finite melt obtained by the numerical simulation (CrysMAS) are compared to the above analytical solution for the infinite melt and disk. Radial (V_r) and axial (V_z) velocities are compared. As can be observed in equations (14), the radial velocity depends on the radius, and the axial velocity only depends on the distance to the disk. The radial velocity are studied at r=0.5R (R=0.006m) and at r=R. The results obtained can be observed in the following figures.

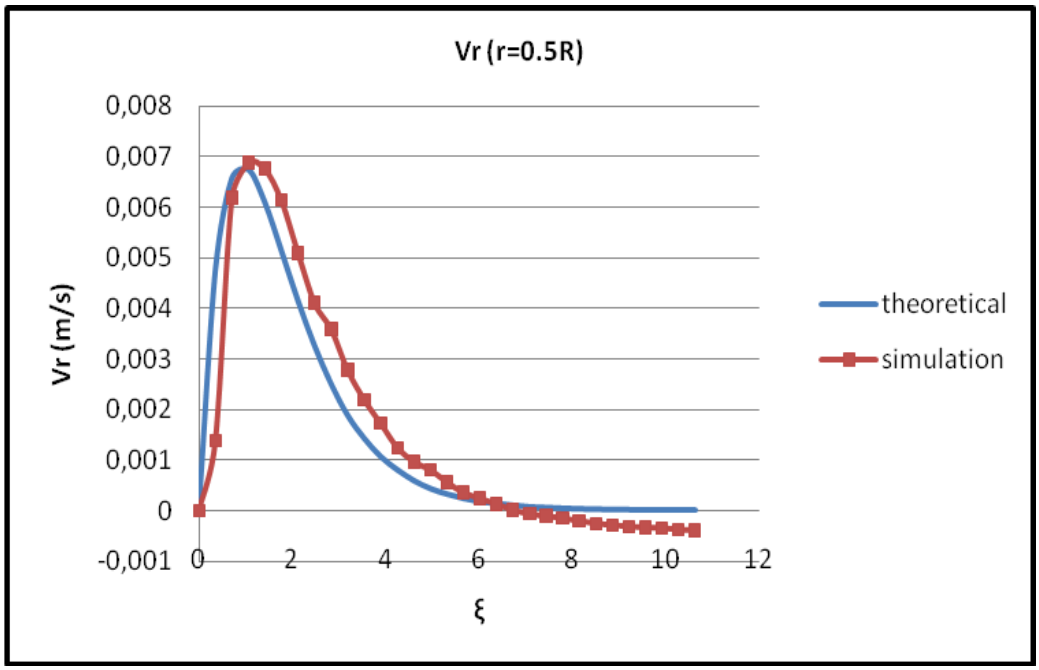

Figure 26. Theoretical and simulated radial velocities at r=0.5R when f=2Hz.

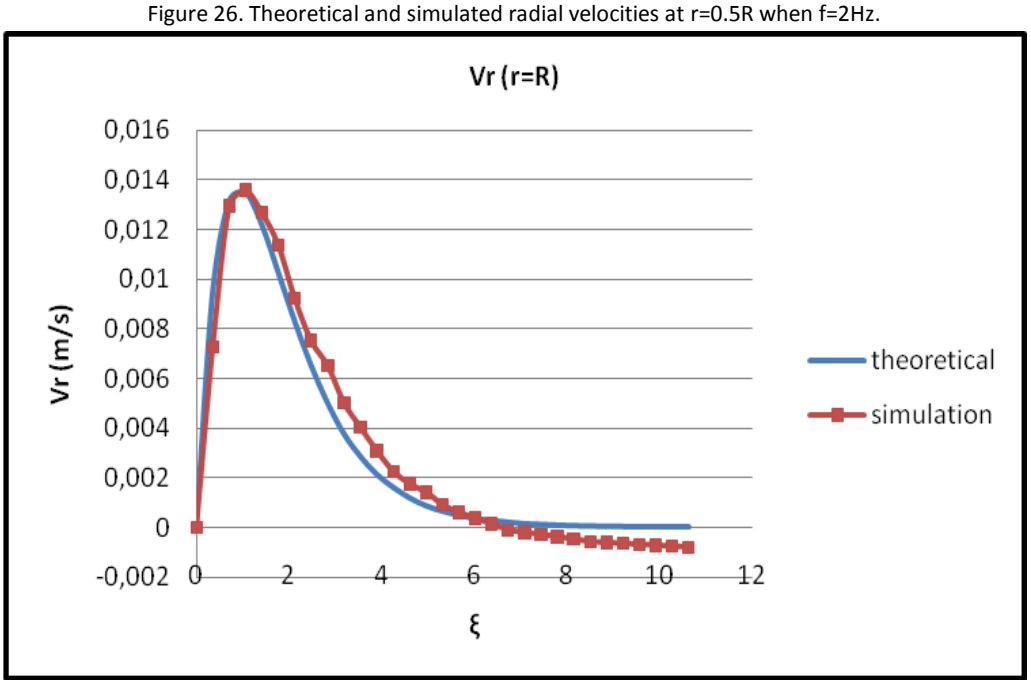

Figure 27. Theoretical and simulated radial velocities at r=R when f=2Hz.

In the simulation, negative values for the radial velocity appear. This phenomena would also happen in a real experiment, and it is due to the non-infinit disk. As it can be observed in Figure 21 and in Figure 22, the flow moves radially outwards.

The axial velocity will be compared at r=0, r=0.5R and r=R, but all are plotted in a single chart, since according to the analytical solution, the axial velocity should not depend on the radial distance.

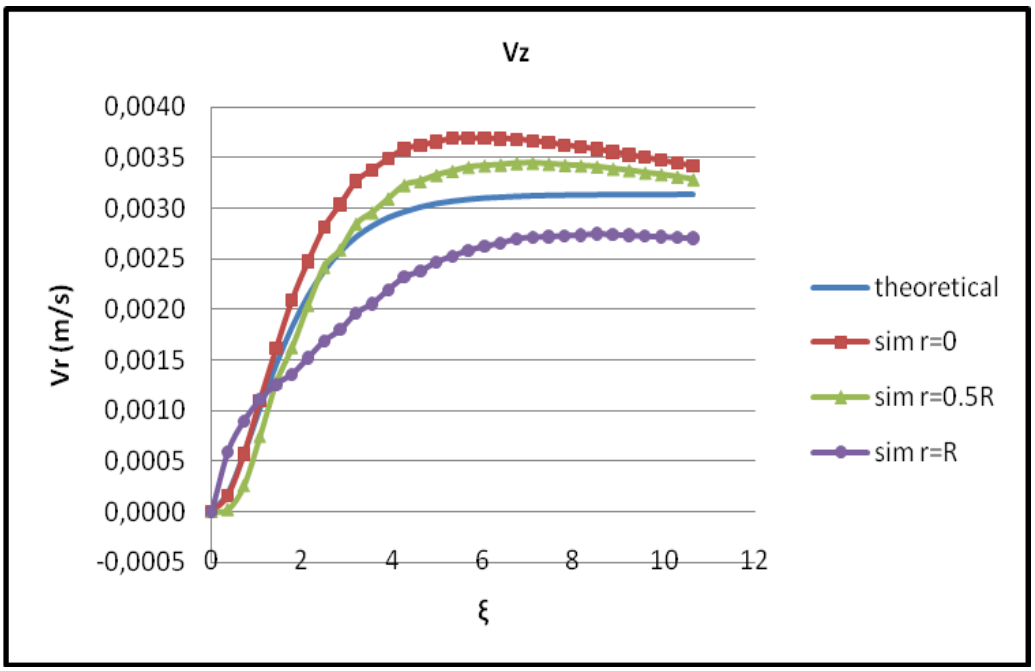

Figure 28. Theoretical and simulated axial velocities at r=0, r=0.5R and r=R when f=2Hz.

It has been proved that the velocities obtained with the simulation are very similar to the theoretical ones. The next step is to set the range of rotation rates that permit this to happen.

12.2. Comparison to analytical solution for infinite rotating disk for f=1Hz

When the frequency of the rotation is reduced from 2Hz to 1Hz, the radial and axial velocities obtained in the melt are the following ones.

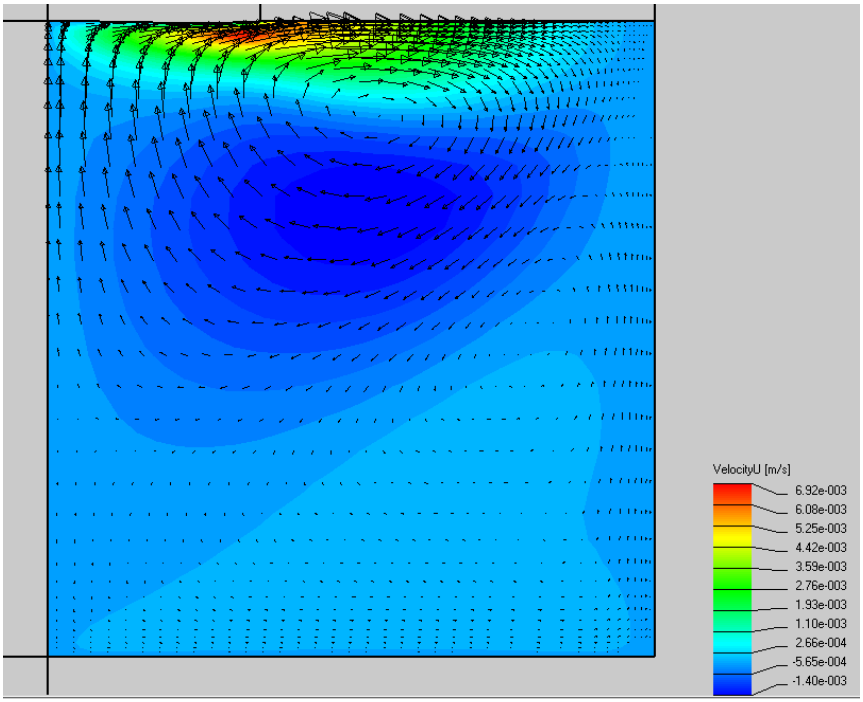

Figure 29. Radial velocities in the melt when the flow is driven by both natural and forced convection, and f=1Hz.

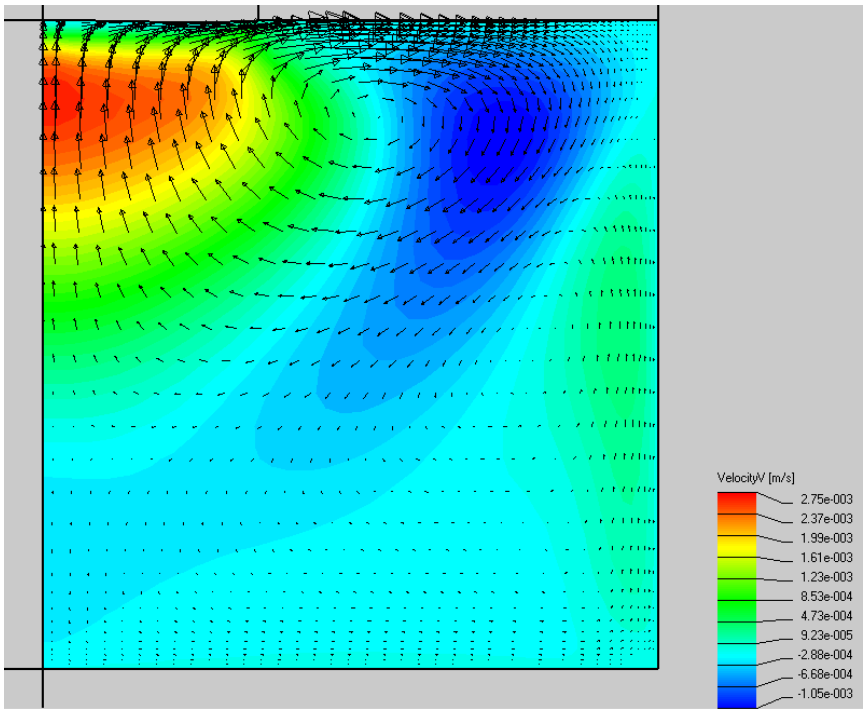

Figure 30. Axial velocities in the melt when the flow is driven by both natural and forced convection, and f=1Hz.

The highest ΔT in the melt is still 2K and the Grashof number has the same value:

$$Gr = 15696$$

The Reynolds number has the following value:

$$\mathrm{Re} = \frac{2 \cdot \pi \cdot 1 \cdot 0.006^2 \cdot 5310}{0.00531} = 226$$

The relation between the Grashof number and the Reynolds number squared is the following one:

$$\frac{\mathrm{Re}^2}{Gr} = \frac{226^2}{15696} = 3.25$$

This value shows that the forced convection still controls the movement of the melt, but the natural convection has more influence than in the previous situation studied. This can be observed in Figure 29 and in Figure 30.

In the next graphics one can see the comparison between the velocities obtained in the melt and the velocities that would be obtained with an infinite rotating disk.

The radial velocities are shown in Figure 31 and Figure 32 and the axial velocities in Figure 33.

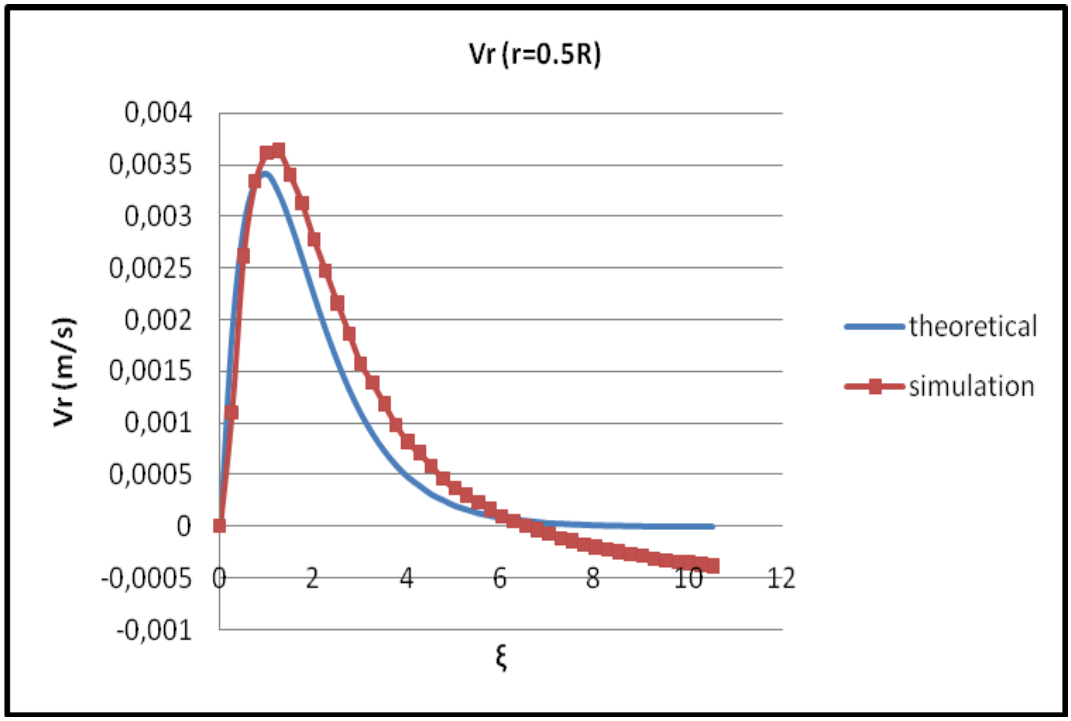

Figure 31. Theoretical and simulated radial velocities at r=0.5R when f=1Hz.

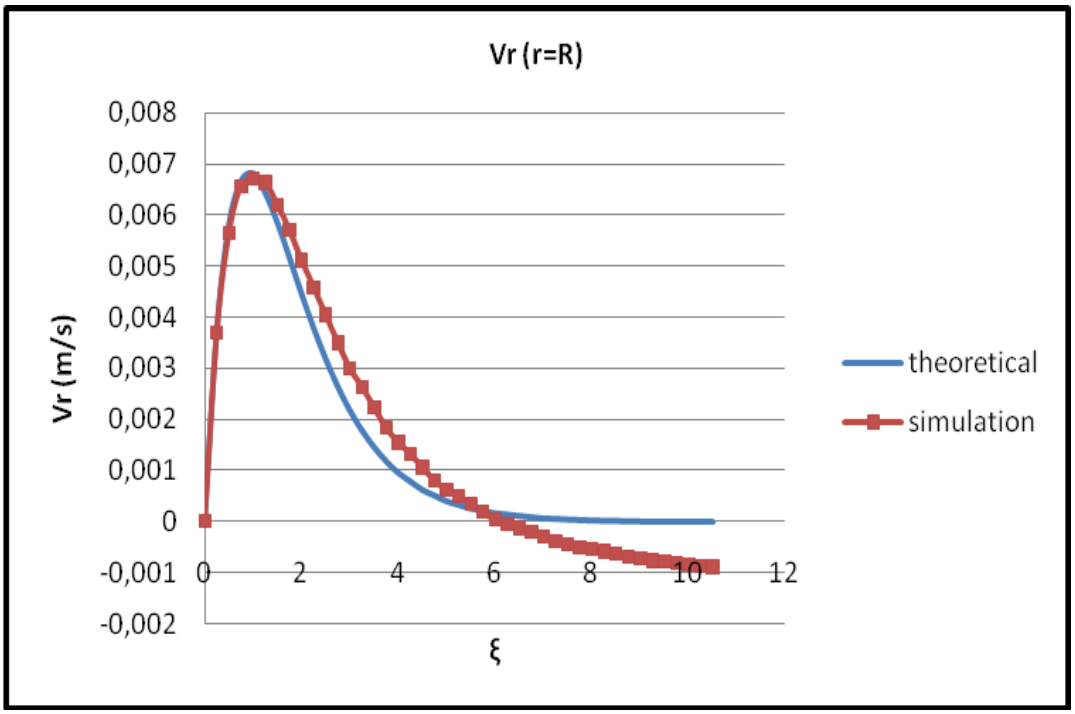

Figure 32. Theoretical and simulated radial velocities at r=R when f=1Hz.

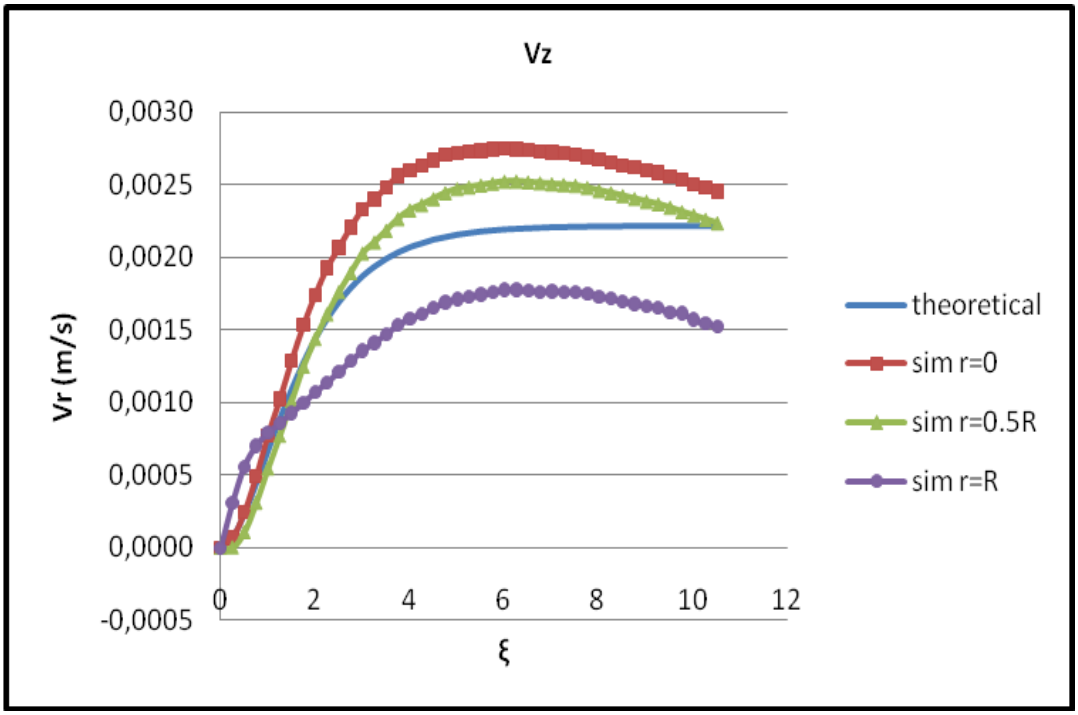

Figure 33. Theoretical and simulated axial velocities at r=0, r=0.5R and r=R when f=1Hz.

12.3. Comparison to analytical solution for infinite rotating disk for $Gr \sim Re^2$

In this section the frequency of the rotation is 0.5Hz. The radial and axial velocities obtained in the melt are the following ones.

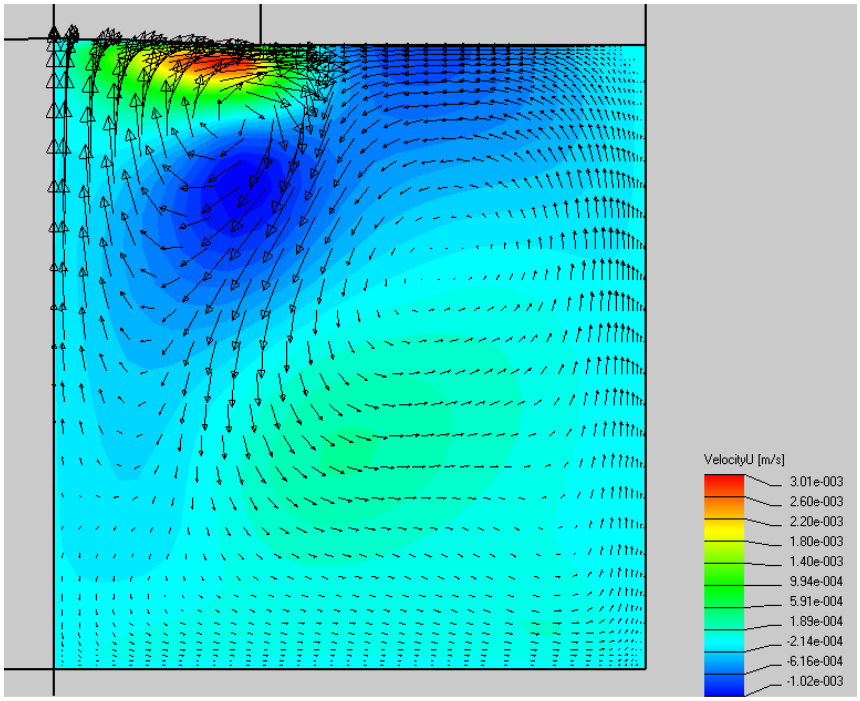

Figure 34. Radial velocities in the melt when the flow is driven by both natural and forced convection, and f=0.5Hz.

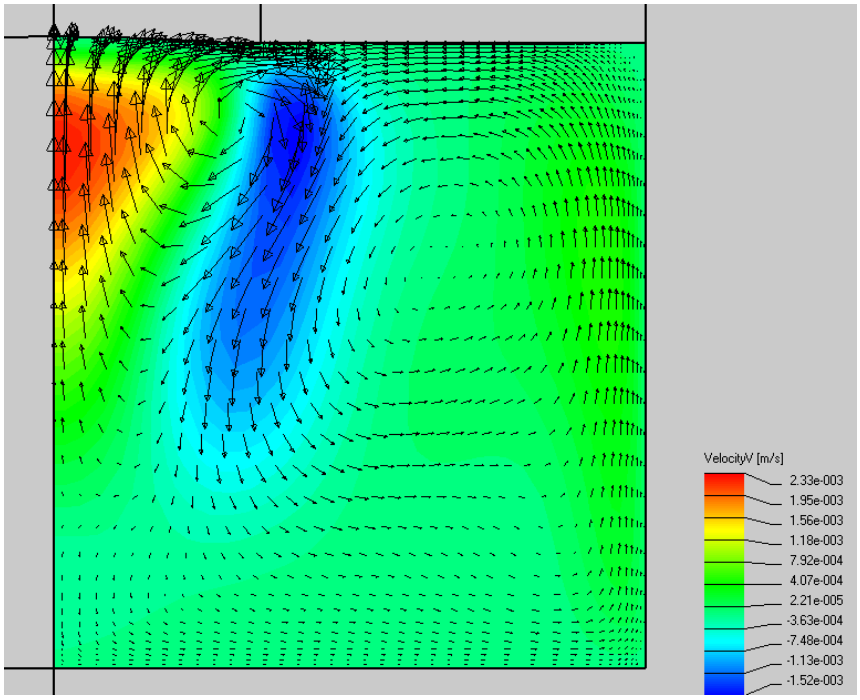

Figure 35. Axial velocities in the melt when the flow is driven by both natural and forced convection, and f=0.5Hz.

The highest ΔT in the melt is still 2K and the Grashof number has the same value:

$$Gr = 15696$$

The Reynolds number has the following value:

$$\mathrm{Re} = \frac{2 \cdot \pi \cdot 0.5 \cdot 0.006^2 \cdot 5310}{0.00531} = 113$$

The relation between the Grashof number and the Reynolds number squared is the following one:

$$\frac{\mathrm{Re}^2}{Gr} = \frac{113^2}{15696} = 0.8$$

This value, Figure 34 and Figure 35 show that, in this situation, the natural convection is as important as the forced convection. When looking at the movement of the melt, it is possible to observe that under the crystal the melt is controlled by the movement of the crystal, that is to say, the forced convection. On the other hand, the rest of the melt is controlled by natural convection, in the same direction than in section 10.

In the next graphics one can see the comparison between the velocities obtained in the melt and the velocities that would be obtained with an infinite rotating disk.

The radial velocities are shown in Figure 36 and in Figure 37 and the axial velocities in Figure 38.

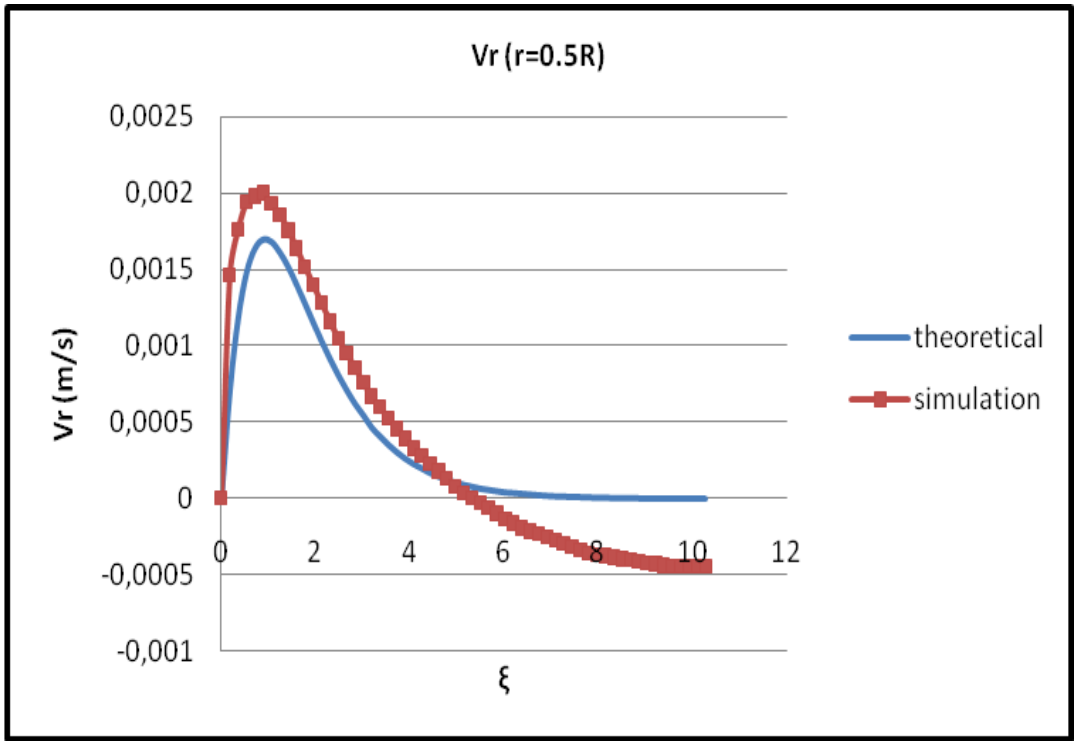

Figure 36. Theoretical and simulated radial velocities at r=0.5R when f=0.5Hz.

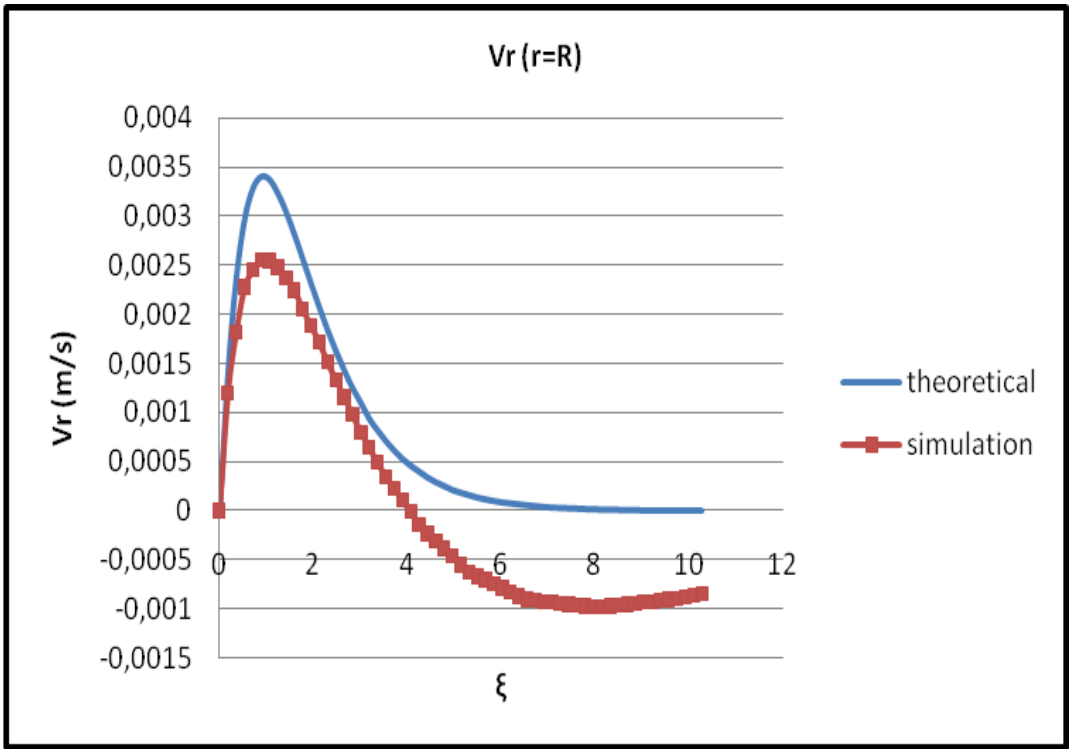

Figure 37. Theoretical and simulated radial velocities at r=R when f=0.5Hz.

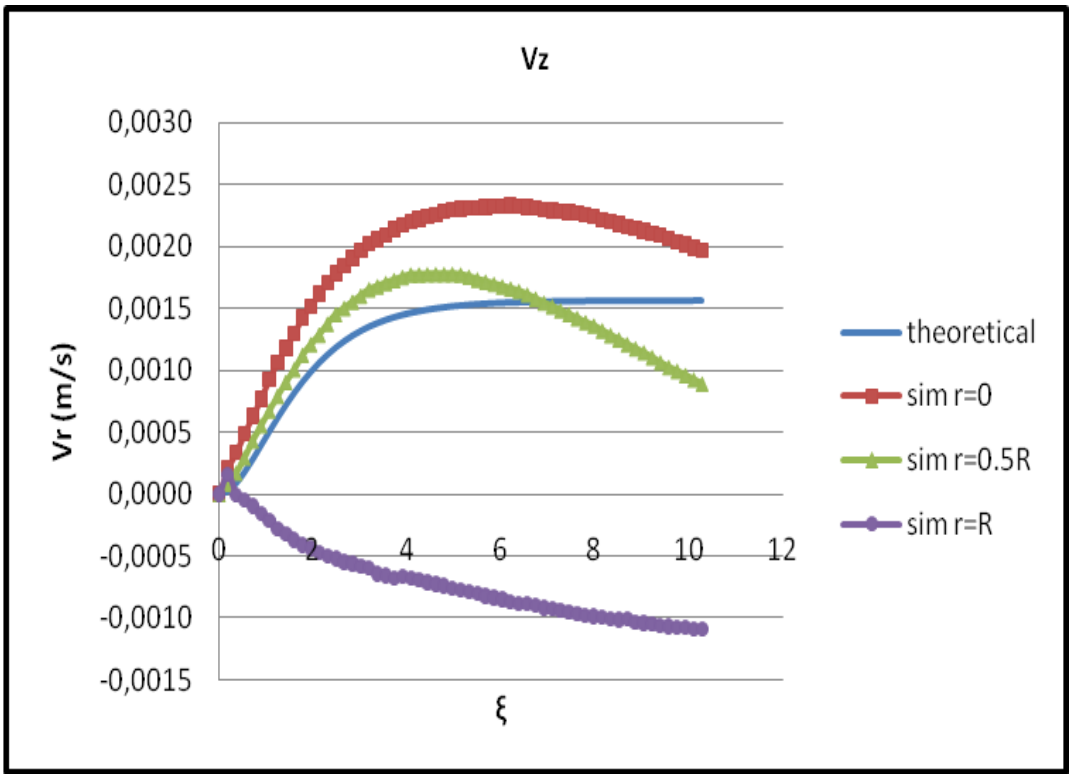

Figure 38. Theoretical and simulated axial velocities at r=0, r=0.5R and r=R when f=0.5Hz.

13. Natural and forced convection with pulling rate

To have the whole Czochralski process simulated, the only thing missing is pulling the crystal, factor that lets the crystal to grow vertically. The pulling rate used is 1mm/h (low velocities are needed) and the rotation rate is kept at 2Hz.

In the following figures, one can observe the temperatures obtained in the system.

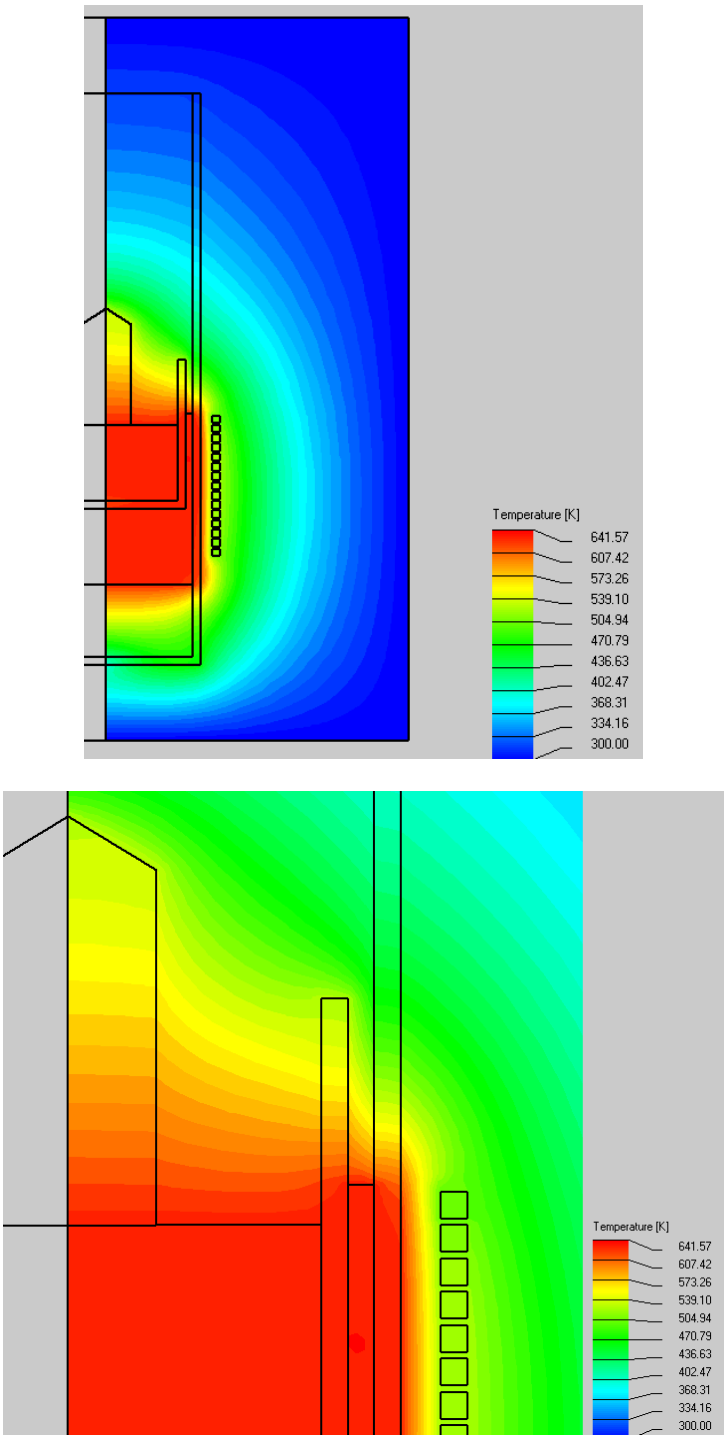

Figure 39. Distribution of temperatures when the flow is driven by both natural and forced convection and the crystal is pulled.

In the following figures, the radial, axial and azimuthal velocities of the melt are shown.

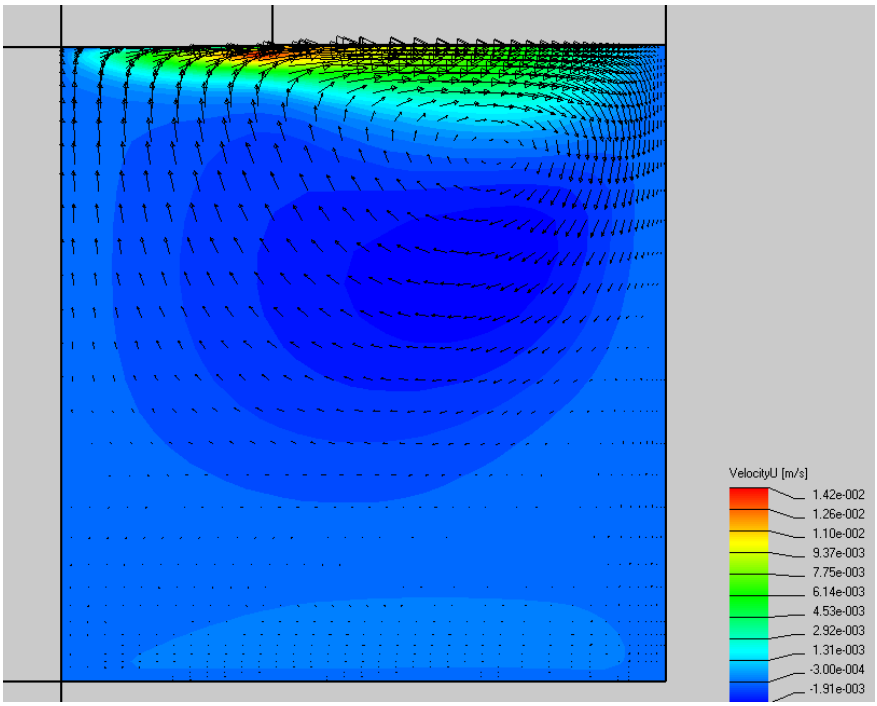

Figure 40. Radial velocities in the melt when the flow is driven by both natural and forced convection and the crystal is pulled.

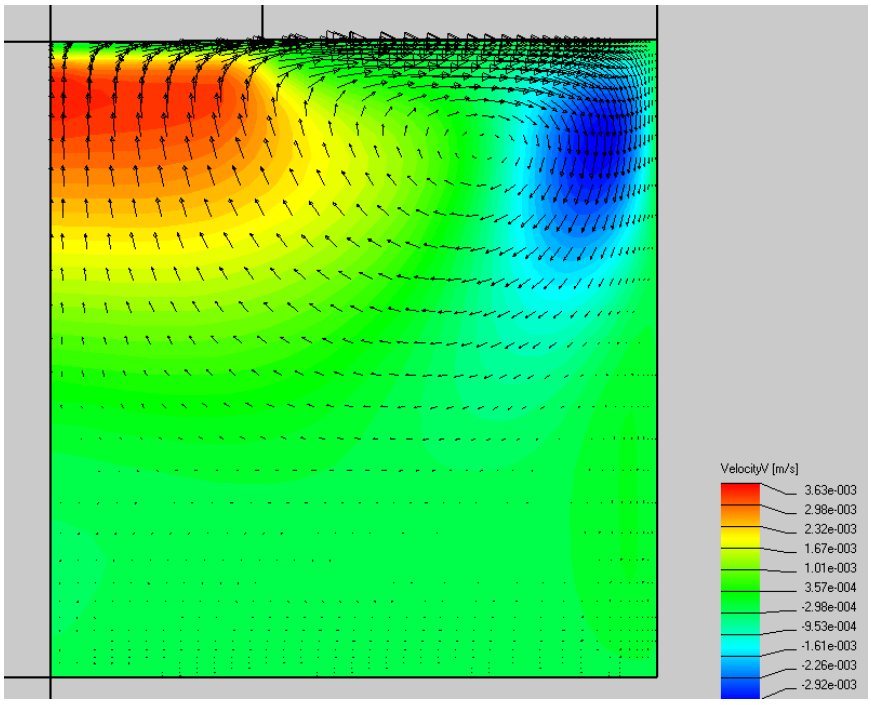

Figure 41. Axial velocities in the melt when the flow is driven by both natural and forced convection and the crystal is pulled.

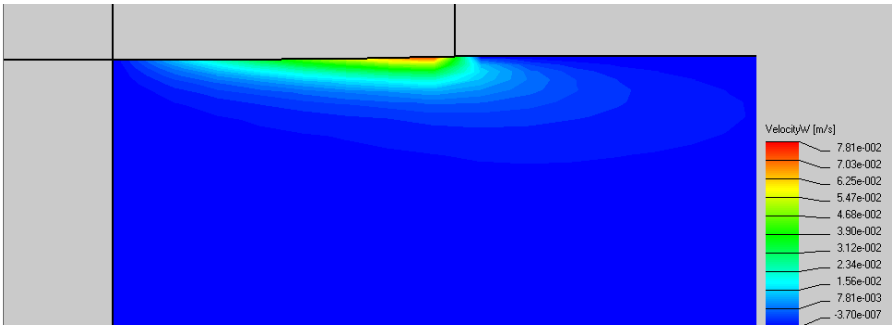

Figure 42. Azimuthal velocities in the melt when the flow is driven by both natural and forced convection and the crystal is pulled.

As one can observe in the previous pictures, pulling up the crystal does not affect to the movement of the melt, the flow still moves outwords. The relation between the Reynolds number and the Grashof needs to be checked.

The highest ΔT in the melt is 1K, so the Grashof number has the following value:

$$Gr = \frac{9.81 \cdot 0.0001 \cdot 1 \cdot 0.02^3 \cdot 5310^2}{0.00531^2} = 7848$$

The Reynolds number has the same value as in the previous case.

$$\mathrm{Re} = \frac{2 \cdot \pi \cdot 2 \cdot 0.006^2 \cdot 5310}{0.00531} = 452$$

The relation studied takes the following value:

$$\frac{\mathrm{Re}^2}{Gr} = \frac{452^2}{7848} = 26$$

so it is possible to conclude that the forced convection still controls the movement of the melt.

The maximum velocities in the melt are the following ones:

$$V_{r\,\max} = 0.0142 m/s$$

$$V_{z\,\max} = 0.00363 m/s$$

$$V_{\theta\,\max} = 0.0781 m/s$$

Reynolds numbers based on these velocities are:

$$\mathrm{Re}_{r,\max} = \frac{V_{r\,\max} D \rho}{\mu} = \frac{0.0142 \cdot 0.02 \cdot 5310}{0.00531} = 284$$

$$\mathrm{Re}_{z,\max} = \frac{V_{z,\max} D\rho}{\mu} = \frac{0.00363 \cdot 0.02 \cdot 5310}{0.00531} = 72.6$$

$$\mathrm{Re}_{\theta,\max} = \frac{V_{\theta,\max} D\rho}{\mu} = \frac{0.0781 \cdot 0.02 \cdot 5310}{0.00531} = 1562$$

It can be concluded that such a small pulling rate does not influence to the values of the velocities. It has not either repercussion on the geometry of the interface, as it is still almost flat. The interface can be observed in Figure 43.

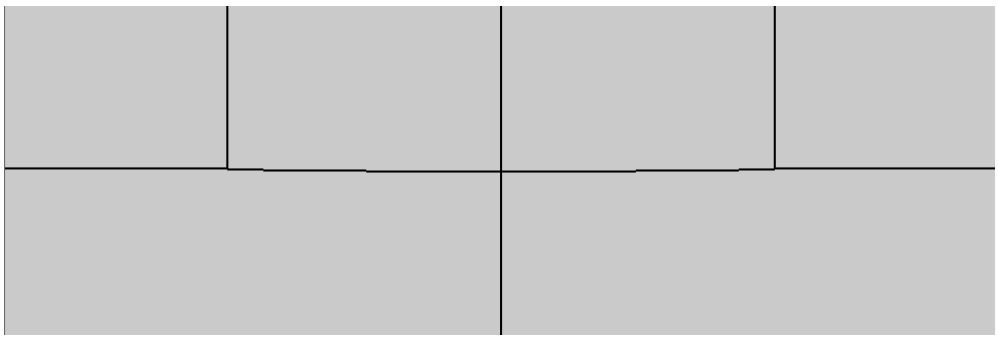

Figure 43. Geometry of the interface when the flow is driven by both natural and forced convection and the crystal is pulled.

14. Summary and conclusions

The heat transfer and fluid flow occurring during the Czochralski process were simulated using CrysMAS code. The growth of InI was considered. InI has an unusually low melting point, which makes the Czochralski growth process difficult. InI is a promising X- and gamma-ray detector material.

The simulation included several steps. First, the geometry was designed, adapting the shapes and sizes of the devices and materials to the features of the program. Once the materials were assigned to each region, the grid was created, making it thinner or structured in the zones that required it. Then the heater, the boundary conditions and the process parameters were defined, according to the power supply available, the thermophysical conditions that the laboratory presents and considering the crystal growth requirements, respectively.

The first simulations were done using the dimensions of the materials and devices available in the laboratory. Due to InI's low freezing point, low temperature gradients were expected in the melt. In order to increase this gradient, the size of the graphite size was modified several times. The length of the piece that produced the highest gradient in the melt was chosen and used for all the simulations in this study.

The distribution of temperatures and the behavior of the melt were studied in different situations. The distribution of temperatures was almost the same in all the situations, small changes could be observed, but the melt behaved differently in the four cases.

The first case considered was natural convection alone driven by buoyancy forces, which produced a flow from the crucible wall towards the crystal, along the surface of the melt. The second case considered was forced convection alone, flow driven by a crystal rotating at 120 RPM. Here the centrifugal forces produced a flow pattern along the melt surface, from the crystal towards the crucible walls. Moreover, the velocities of the melt were much higher when the flow was driven by forced convection.

The third case considered was mixed convection, driven by both buoyancy and centrifugal forces. In this case, the goal was to set the rotation rate of the crystal sufficiently high to ensure that the forced convection had more influence on the melt flow than the natural convection. This was verified by observing the flow pattern, which was similar to the one produced by the forced convection alone, and also using nondimensional parameters.

The fourth situation studied was the most realistic case, including the translation of the growing crystal (the pulling rate of the crystal was set to 1mm/h) and the mixed convection in the melt (both natural and forced convection occurring together). Introducing the pulling rate did not change significantly the flow pattern and the velocities in the melt.

Finally, the radial and axial velocities obtained when there were both natural and forced convection were compared to the analytical solution for the infinite rotating disk. The values obtained with the CrysMAS simulation were very similar to the analytical solution. Yet, there were two significant differences:

(i) In the CrysMAS simulation, the radial velocities in the furthest positions from the crystal were negative. This is because the volume studied was not infinite and there was recirculation. In the theoretical situation, the disk is infinite and the recirculation occurs in the infinity.

(ii) The second difference was in the axial velocities, when the distance from the center of the melt was equal to the radius of the crystal. As this is the point when the flow loses the contact with the surface of the crystal, the velocities were a bit lower than the theoretical ones. However, they had the same evolution.

After checking the good correspondence between the results of the simulation and the analytical solution, the range of velocities for which this correspondence was possible was studied. Two more values for the rotation rate were studied.

a) The frequency was reduced to 1Hz (1/2 of the initial value). The agreement was still acceptable. The forced convection was still controlling the flow, but the natural convection gained influence. This caused that the negative values of the radial velocity were higher (in absolute value), and also caused a higher difference between the analytical axial velocities at the end of the crystal and the values obtained from the simulation.

b) Finally, the frequency was reduced to ¼ of the initial value. This made the natural convection as important as the forced convection. With this value, the melt under the crystal was controlled by the movement of the crystal, and the rest of the melt was controlled by buoyancy forces. When comparing the radial velocities, it was possible to observe that the negative values were more negative than in the other situations. The axial velocities were more different to the theoretical ones than before, overall the velocities at the end of the crystal. These velocities were all negative, because at this point the natural convection controlled the flow.

It can be concluded that the Cochran's analytical solution for the infinite rotating disk predicts accurately the flow in Czochralski melts, provided that the flow is dominated by crystal rotation, $\mathrm{Re}^2 >> Gr$ (where Re is the rotational Reynolds number, based on the crystal rotation rate and diameter, and r is the Grashof number of the melt).

15. References

[1] T. Onodera, K. Hitomi, T. Shoji, Fabrication of indium iodide X- and gamma-ray detectors, IEEE Transactions on nuclear science 53 (5) (2006) 3055.

[2] K.S. Shah, P. Bennett, L.P. Moy, M.M. Misra, W.W. Moses, Characterization of indium iodide detectors for scintillation studies, Nuclear Instruments and Methods in Physics Research A 380 (1996) 215.

[3] P. Bhattacharva, M. Groza, Y. Cui, D. Caudel, T. Wrenn, A. Nwankwo, A. Burger, G. Slack, A.G. Ostrogorsky, Growth of InI single crystals for nuclear detection applications, Journal of Crystal Growth 312 (2010) 1228.

[4] A.G. Ostrogorsky, personal communication.

[5] U. Krzyminsky, A.G. Ostrogorsky, Visualization of convection in Czochrralski melts using salts under realistic thermal boundary conditions, Journal of Crystal Growth 174 (1997) 19.

[6] M.H. Tavakoli, H. Wilke, Numerical study of induction heating and heat transfer in a real Czochralski system, Journal of Crystal Growth 275 (2005) e85.

[7] W.G. Cochran, The flow due to a rotating disk, Proc. Cambridge Phil. Soc., 30 (1934) 365.

[8] T. von Kármán, Über laminare und turbulente Reibung, Z. Angew Math Mech. 1 (1921) 233.

[9] P.M. Gresho, J.J. Derby, A finite element model for induction heating of a metal crucible, Journal of Crystal Growth 85 (1987) 40.

[10] M.H. Tavakoli, Numerical study of heat transport and fluid flow during different stages of sapphire Czochralski crystal growth, Jounal of Crystal Growth 310 (2008) 3107.

[11] F.M. White, Viscous fluid flow, McGraw-Hill series in mechanical engineering (1991)

[12] M.H. Tavakoli, E. Mohammadi-Manesh, A. Ojaghi, Influence of crucible geometry and position on the induction heating process in crystal growth systems, Journal of Crystal Growth 311 (2009) 4281.

[13] D. Gasperino, M. Bliss, K. Jones, K. Lynn, J.J. Derby, On crucible effects during growth of cadmium zinc telluride in an electrodynamic gradient freeze furnace, Journal of Crystal Growth 311 (2009) 2327.

[14] D. Schulz, S. Ganschow, D. Klimm, K. Struve, Inductively heated Bridgman method for the growth of zinc oxide single crystals, Journal of Crystal Growth 310 (2008) 1832.

16. Acknowledgments

This project has been done with the collaboration of Jon Agirre Gonzalez (DNI 72508034-M), I am grateful for his contribution.

I deeply thank my advisor, Professor Aleksandar Ostrogorsky, for his supervision and advice.

Finally, I would like to thank my family, specially my mother and my brothers, because without them this project would not have been possible.